JOURNAL OF GEOPHYSICAL RESEARCH, VOL. 99, NO. A11, PAGES 21,257–21,280, NOVEMBER 1, 1994

Statistical characteristics of bursty bulk flow events

V. Angelopoulos,[1,2,5] C. F. Kennel,[1,2] F. V. Coroniti,[1] R. Pellat,[1] M. G. Kivelson,[2]
R. J. Walker,[2] C. T. Russell,[2] W. Baumjohann,[3] W. C. Feldman,[4] and J. T. Gosling[4]

Abstract. Using a common methodology to analyze data from the AMPTE/IRM and ISEE 2 satellites we report on the statistical properties of bursty bulk flow events (BBFs) in the inner plasma sheet (IPS). A positive correlation between BBFs and the AE index suggests that BBFs are predominantly geomagnetically active time phenomena. Earthward BBFs are more frequent close to midnight and away from Earth, up to a distance of ~19 R_E. Tailward BBFs are very infrequent in the IRM data set and somewhat less infrequent in the ISEE 2 data set in the region of the satellites' spatial overlap, possibly due to the more active conditions prevailing during the ISEE 2 mission in that region. However, in both data sets the ratio of tailward to earthward BBFs increases with distance from Earth; more than 20% of all BBFs are anti-sunward tailward of $X = -19\ R_E$ in the ISEE 2 data set. BBFs are responsible for 60-100% of the measured earthward transport of mass, energy and magnetic flux past the satellite in the regions of maximum occurrence rate, even though they last approximately 10-15% of the IPS observation time there. Thus BBFs represent the primary transport mechanism at those regions. The one-to-one correspondence between BBFs and substorm phase, as well as the relative contribution of BBFs to the total transport observed during substorms are questions that await further investigation based on multi instrument studies of individual events.

1. Introduction

The data obtained from the Active Magnetospheric Particle Tracer Explorer / Ion Release Module (AMPTE/IRM) satellite have made it possible to reconsider and extend the findings of earlier missions in the near-Earth magnetotail [*Baumjohann*, 1993]. From the point of view of magnetospheric circulation of particles and magnetic flux, as well as plasma sheet heating and energy transport, an important step was made with the report and statistical investigation of a small subset of all AMPTE/IRM plasma sheet samples, namely the high speed flow samples. Although in all plasma sheet regions slow flows dominate [*Baumjohann et al.*, 1988, 1989], the nearly stagnant plasma flow is interrupted by high speed flow bursts of a typical peak-velocity duration of less than 10 s. The flow bursts are directed predominantly earthward. They are associated with relatively low plasma density in all plasma sheet regions and are positively correlated with geomagnetic activity. Their occurrence frequency increases with proximity to local midnight and with distance away from Earth. *Baumjohann et al.* [1990] defined the inner central plasma sheet (ICPS) as the region where $B_{xy} = \left(B_x^2 + B_y^2\right)^{1/2} <$ 15 nT, or $B_x/B_{xy} > 0.5$ and the plasma sheet boundary layer (PSBL) as the region where photoelectrons enhance the electron density above the ion density ($N_e > N_i^{0.86}$). They showed that 400-600 km/s speed flows occur within the ICPS and PSBL in a 1:2 ratio; for flows above 800 km/s this ratio becomes 1:1. Thus the vicinity of the neutral sheet was found to be quite dynamic in the AMPTE/IRM data set, contrary to conclusions based primarily on data from the ISEE satellites [*Eastman et al.*, 1985]. In addition, the direction of the bursts of plasma flow in the ICPS is predominantly across the instantaneous magnetic field, rendering them possible significant contributors to the total measured magnetic flux transport.

The high speed flows in the ICPS were studied on a case-by-case basis by *Angelopoulos et al.* [1992a]. The authors concluded that the rise-and-fall timescale of the flow bursts is of the order of a minute and that the bursts occur within 10-min timescale flow enhancements termed bursty bulk flow events (BBFs). The bursts of flow are associated with ion heating and plasma sheet dipolarization. In a statistical study of BBFs in the AMPTE/IRM data set, *Angelopoulos et al.* [1992b] showed that such events are relatively infrequent (< 7% of the time in the plasma sheet and < 20% of the time in the ICPS) but can produce roughly half of the earthward mass and energy transport measured past the satellite during its 1985 magnetotail passes and most of the earthward magnetic flux transport. Thus such events represent important building blocks of magnetotail transport.

High speed flows in the near-Earth central plasma sheet (CPS) have been reported in the past, in particular in data from the ISEE satellites [e.g., *Hones*, 1979; *Nishida et al.*, 1981; *Cattell and Mozer*, 1984; *Huang et al.*, 1987; *Ohtani et al.*, 1992; *Sergeev et al.*, 1992]. However, such flows have received little attention from the point of view of transport because they were thought to be statistically insignificant based on the low average flow velocity in the CPS regardless of geomagnetic activity [*Huang and Frank*, 1986, 1987]. The CPS was defined by *Huang and Frank* [1986, 1987] by the exclusion of other magnetotail regions: If the ion bulk speed V_i was greater than 150 km/s, the flow was tailward and the density N_i was greater than 1 cm^{-3} the sample was excluded as a low-latitude boundary layer sample; if $N_i < 10^{-2}$ cm^{-3} and the ion bulk flow was tailward the sample was excluded as a lobe sample; if $V_i > 150$ km/s and the spacecraft was more than

[1]Department of Physics, University of California, Los Angeles.
[2]Institute of Geophysics and Planetary Physics, University of California, Los Angeles.
[3]Max-Planck-Institut für Extraterrestrische Physik, Garching, Germany.
[4]Los Alamos National Laboratory, Los Alamos, New Mexico.
[5]Now at the Applied Physics Laboratory, Johns Hopkins University, Laurel, Maryland.

Copyright 1994 by the American Geophysical Union.

Paper number 94JA01263.
0148-0227/94/94JA-01263$05.00

1.5 R_E away from the nominal neutral sheet position the sample was excluded as a plasma sheet boundary layer sample. The realization that the average velocity is small not just in the central plasma sheet but in all plasma sheet regions [*Baumjohann et al.*, 1989] and the importance of AMPTE/IRM BBFs for magnetotail transport raises the issue of whether the apparent differences in impression gained from the AMPTE/IRM and the ISEE 2 data sets regarding earthward transport are attributable to (1) the methodologies used to analyze these data sets, (2) the orbital characteristics of and geomagnetic conditions during the two missions, or (3) the different instruments used to collect the data sets.

Enhanced, impulsive particle and magnetic flux transport is expected in the magnetotail during geomagnetically active times, since at those times the solar wind-imposed dawn-dusk electric field increases [*Kivelson*, 1976], and injection of hot magnetospheric plasma is taking place at geosynchronous altitudes in an impulsive way [*Mauk and Meng*, 1987]. Magnetospheric substorms are an important constituent of our current phenomenological picture of how such transport is accomplished [*McPherron*, 1991]. Indeed, reports of an association of fast plasma sheet flows (and thus enhanced transport) during substorms abound in the literature [e.g., *Hones*, 1979, *Nishida et al.*, 1981; *Cattell and Mozer*, 1984, *Sergeev et al.*, 1992]. Emphasis has been placed on fast tailward plasma sheet flows especially when those are correlated with southward B_z. Such flows have been interpreted as evidence for the existence of a neutral line forming earthward of the observation point [e.g., *Hones*, 1979 and references therein].

An early statistical study of IMP 6 data by *Hayakawa et al.* [1982] had pointed out the existence of fast tailward flows in good correlation with southward B_z in the mid-tail (X = -25 to -30 R_E) plasma sheet. The fast flow ($|V| > 300$ km/s) events of that study are roughly comparable to the BBF events defined by *Angelopoulos et al.* [1992a], the only difference being that near-neutral sheet events were defined by their distance from a model neutral sheet. Out of the 90 fast flow events identified, 20 were tailward; of those tailward fast flow events 75% had an average B_z that was southward. Using IMP 6, 7 and 8 satellite data restricted to neutral sheet encounters, *Nakamura et al.* [1994] confirmed the results of *Hayakawa et al.* [1982] regarding the occurrence rates of fast tailward flow events and their association with southward B_z. *Hones and Schindler* [1979] focused on the subset of the IMP 6 and 8 satellite data sets that is associated with substorm times. They showed that in 50% of the selected substorm intervals, the satellite observed a flow enhancement at around substorm onset; 80% of the time that enhancement was in the tailward direction. This led them to the conclusion that during substorm onset a neutral line forms most frequently earthward of X = -25 to -30 R_E, whereas they interpreted the lack of a flow enhancement in the plasma sheet during the other 50% of their substorm data set as evidence of cross-tail localization of the effects of substorms in space.

Closer to Earth, the most probable location of a possible neutral line during substorm onset is still a point of controversy. A statistical analysis of EXB flows inferred from the electric and magnetic field measurements on ISEE 1 [*Cattell and Mozer*, 1984] had placed the existence of a neutral line most frequently tailward of ~22 R_E, the apogee of the ISEE satellites. Tailward flows, as well as "near-satellite reconnection" events encompassing tailward followed by earthward flows were also present in their data set (comprising 25% of their events) but they were located tailward of X = -21 R_E. Recently, *Kettmann et al.* [1993a, 1993b] analyzed high anisotropy samples (HAS) of energetic (>25 keV) ion data from the ISEE 2 satellite and showed that tailward anisotropies can indeed occur in the plasma sheet with significant occurrence probability as close to Earth as 16 R_E. Although they did not distinguish between boundary layer and neutral sheet HAS samples, they showed that earthward HAS correlate with positive B_z and tailward HAS samples with negative B_z, beyond 16 R_E downtail. They suggested that a near-Earth neutral line may form quite frequently well within the ISEE apogee. The above studies inferred the flow properties within the ISEE apogee based on information other than direct plasma measurements. Their seemingly contradictory results are not very surprising given the different techniques employed to infer the position of a neutral line and the different methodologies applied to select their data sets [*Kettmann et al.*, 1993a].

A statistical analysis of the occurrence rates of fast flows in the ICPS by *Baumjohann et al.* [1989, 1990] revealed a lack of any fast tailward flows in the AMPTE/IRM data set in disagreement with previous case studies of tailward flows in the ISEE data set [e.g., *Paschmann et al.*, 1985b; *Hones et al.*, 1986] from roughly the same region of space. Thus although the discrepancy in the results of *Cattell and Mozer* [1984] and *Kettmann et al.* [1993a] could conceivably be resolved based on methodological differences, the lack of directly measured tailward flows in the AMPTE/IRM data set in a tail region previously reported to support such flows is an issue that still remains unresolved and necessitates a systematic comparison of the AMPTE/IRM and ISEE 2 plasma data, in particular in the region of common coverage.

In this paper we will address the above issues by studying the AMPTE/IRM and ISEE 2 data sets with a common methodology. We will apply the same criteria to distinguish between different plasma sheet regions and will define BBFs in the same computer-automated way. This approach was applied to a study of the non-BBF (quiet) flow in the plasma sheet by *Angelopoulos et al.* [1993]. The similarity of the average quiet flow pattern in the two data sets (their Figure 1), as well as the near-quantitative agreement of the average pressure in the regions sampled by both spacecraft (their Figure 4 (c)) give us further confidence that the two data sets are commensurate. Our analysis will complement the study of *Angelopoulos et al.* [1993] by intercomparing the two data sets during intervals of plasma sheet activity. We will assume that the differences between the two data sets with respect to their temporal resolution and the instrumentation used to acquire them do not, to first order, preclude us from directly intercomparing them. Thus we will attempt to judge whether the results obtained from the two data sets can be understood based on the satellites' orbital biases and the geomagnetic activity during the period of coverage.

By virtue of their definition (to be given in section 4), BBFs occur primarily in the plasma sheet regions closest to the neutral sheet. Contrary to PSBL high speed flows which may map to distant equatorial activations downtail of the observation point, BBFs represent local near-neutral sheet acceleration. Consequently, we can study their spatial distribution without the need of a procedure to map the accelerated flows to their downtail origin.

The plasma sheet may be occasionally inactive (i.e., devoid of high speed flows) during geomagnetically active times [*Hones and Schindler*, 1979, Table 2] and active during geomagnetically quiet times based on the AE index [*Baumjohann et al.*, 1990; *Angelopoulos et al.*, 1992a]. In addition, as pointed out by *Angelopoulos et al.* [1992b] and will be demonstrated again in

section 4, there are no apparent differences between geomagnetically quiet time (as defined by AE) BBFs and geomagnetically active time ones. These observations suggest that the AE index may not be always a good monitor of the instantaneous and local transport conditions in the plasma sheet. For these reasons, and in the spirit of our earlier work [*Angelopoulos et al.*, 1992a, 1993] we will not emphasize the association of plasma sheet transport with AE but rather attempt to characterize impulsive plasma sheet transport in its own right, i.e., in terms of BBFs. Naturally, we will try to place BBFs in the context of the measured geomagnetic activity statistically, but we will leave the direct association of BBFs and AE for detailed, multiinstrument case studies that are better suited to remove ambiguities between the two activity indicators.

In section 2 we describe the data sets used in this study. In section 3 we explain the criteria used to define the inner and outer plasma sheet regions (IPS and OPS respectively). Section 4 presents detailed observations of tailward and earthward BBFs in the ISEE 2 data set and an earthward BBF in the IRM data set. Section 5 addresses the spatial dependence of the BBF occurrence rates in the two data sets. The subset of tailward BBFs and fast tailward flow samples is studied in greater detail in this section. Section 6 deals with the importance of BBFs for transport. A summary and discussion is presented in the last section.

2. Data Sets

The analysis presented in this paper was based on 5 s resolution plasma moments from the three dimensional plasma instrument [*Paschmann et al.*, 1985a] and magnetic field data from the fluxgate magnetometer [*Lühr et al.*, 1985] on AMPTE/IRM from the 1985 magnetotail crossings (January 23, 1985 to June 31, 1985). We also used plasma moments from the Los Alamos/Max-Plank-Institut Fast Plasma Experiment (FPE) [*Bame et al.*, 1978] and magnetic field data from the University of California, Los Angeles fluxgate magnetometer [*Russell*, 1978] on ISEE 2 from the 1978 and 1979 magnetotail crossings (December 26, 1977 to June 30, 1978 and December 31, 1978 to June 6, 1979). The FPE plasma data were calculated at 3-s or 12-s resolution depending on the orbit. They were block averaged with a 12 s window and were merged with magnetic field data of the same temporal resolution. The ISEE 2 orbit extended our analysis beyond the apogee of IRM (19 R_E), out to 22 R_E, and complemented AMPTE/IRM's limited coverage in the postmidnight sector.

We transformed the satellite position in an Aberrated Geocentric Solar Magnetospheric (AGSM) system using a 4.5° aberration angle. We limited our databases to be outside the hinge point region [*Hammond et al.*, 1994], $X_{AGSM} < -10\ R_E$. We also confined our analysis to the region $|Y_{AGSM}| < 15\ R_E$ in order to avoid crossings of the magnetopause. In addition, we eliminated other possible magnetopause boundary crossings by searching for times during which the ion temperature T_i dropped below 500 eV, the ion density N_i increased beyond 1 cm^{-3} and the flow was persistently (>5 min) tailward (>200 km/s) at distances of $|Y| > 10\ R_E$. These were removed based on the times of the rotation of the field from the magnetospheric to the magnetosheath direction. Mantle crossings were also removed from the region $\left(Y^2_{AGSM}+Z^2_{AGSM}\right)^{\frac{1}{2}} > 10R_E$ and $Z_{AGSM} > 6R_E$ based on the same criteria as the potential magnetopause crossings.

3. Identification of Plasma Sheet Regions

The definition of PSBL used by *Baumjohann et al.* [1988] (described in the introduction) was particular to the AMPTE/IRM data set, because it used the fact that photoelectrons were not removed from the electron distributions prior to the calculation of the electron moments. Thus, differences between the ion and electron densities on AMPTE/IRM were mostly due to an abundance of photoelectrons at the low density and temperature plasma of the PSBL. However, a similar criterion could not be applied to the ISEE 2 data set without significant effort, because of the different way that the electron moments were calculated from the raw counts of the FPE instrument. In addition, the photoelectron current that influences the detector response to the ambient plasma conditions is a complicated function of several satellite parameters [*Garrett*, 1981] and is expected to be different for the two satellites. Thus a direct intercomparison of the data sets would require careful intercalibration of the two satellites. We wished to devise spacecraft-independent criteria to separate regions within the plasma sheet. Furthermore, *Baumjohann et al.* [1990] defined the ICPS using a magnetic field elevation-dependent criterion. Since BBFs correlate with dipolarizations (temporal increases of B_z), it is possible that a correlation of BBFs with dipolarizations could arise in a statistical study simply from the ICPS selection criterion. We needed to define the regions closest to the neutral sheet based on criteria other than the elevation of the magnetic field or the value of B_z, which are some of the quantities that we intended to study.

To identify lobe samples we used the measured ion pressure P_i (also see *Chen and Kivelson* [1991]) hereby defined as $N_i kT_i$ where k is the Boltzman constant. For the ISEE 2 data set we used $T_i = (T_{parmax} + T_{permin})/2$ where T_{parmax} is the maximum ion temperature encountered during a spin of the spacecraft and T_{permin} is the temperature in the direction perpendicular to that of the maximum temperature. Figures 1(a) and 2(a) are scatterplots of the IRM and ISEE 2 data sets, after a decimation by a factor of 10 (i.e., plotting every tenth sample to reduce the size of the file), in a P_i-H_{NS} space. H_{NS} is the distance from the neutral sheet as defined by *Hammond et al.* [1994]. Two clusters of points appear in this space: a high pressure, low H_{NS} cluster, presumably composed of plasma sheet samples, and a low pressure, high H_{NS} cluster, presumably composed of lobe samples. The values of P_i in the low pressure, high elevation cluster are comparable to the apparent noise level of the instruments in the magnetotail lobes based on case studies. The ion pressure histograms at the bottom of the scatterplots in Figures 1(a) and 2(a) reveal the existence of a minimum between the high pressure and the low pressure clusters of points. Individual cases suggest that this minimum appears because when the spacecraft exits the plasma sheet the plasma instrument quickly attains its apparent noise level, which is quite lower than the pressure values in the plasma sheet. We defined the level of $P_i = 0.01$ nPa to be the dividing line between lobe and plasma sheet regions for both instruments. This is a value chosen conservatively to avoid any possible lobe sample contamination of the plasma sheet data set. Our criterion is also close to the X-dependent criterion used by *Chen and Kivelson* [1991] (e.g., for X = -15 R_E their lobe criterion was equivalent to $P_i < 0.4 \times 10^{-2}$ nPa). Samples with $P_i < 0.01$ nPa are considered as lobe samples in the following.

To develop criteria that separate regions within the plasma sheet, we needed to focus on quantities that can function as indicators of distance from the neutral sheet. The ratio of thermal to magnetic pressure β_i is one such quantity. Another is the magnetic field vector elevation angle above the equatorial plane $\theta_{el} = \text{atan}\,(B_z/(B^2_x + B^2_y)^{1/2})$. As explained earlier, we needed to dissociate our selection criteria from θ_{el} in order to study the correlation of BBFs and dipolarizations. However, a scatterplot of

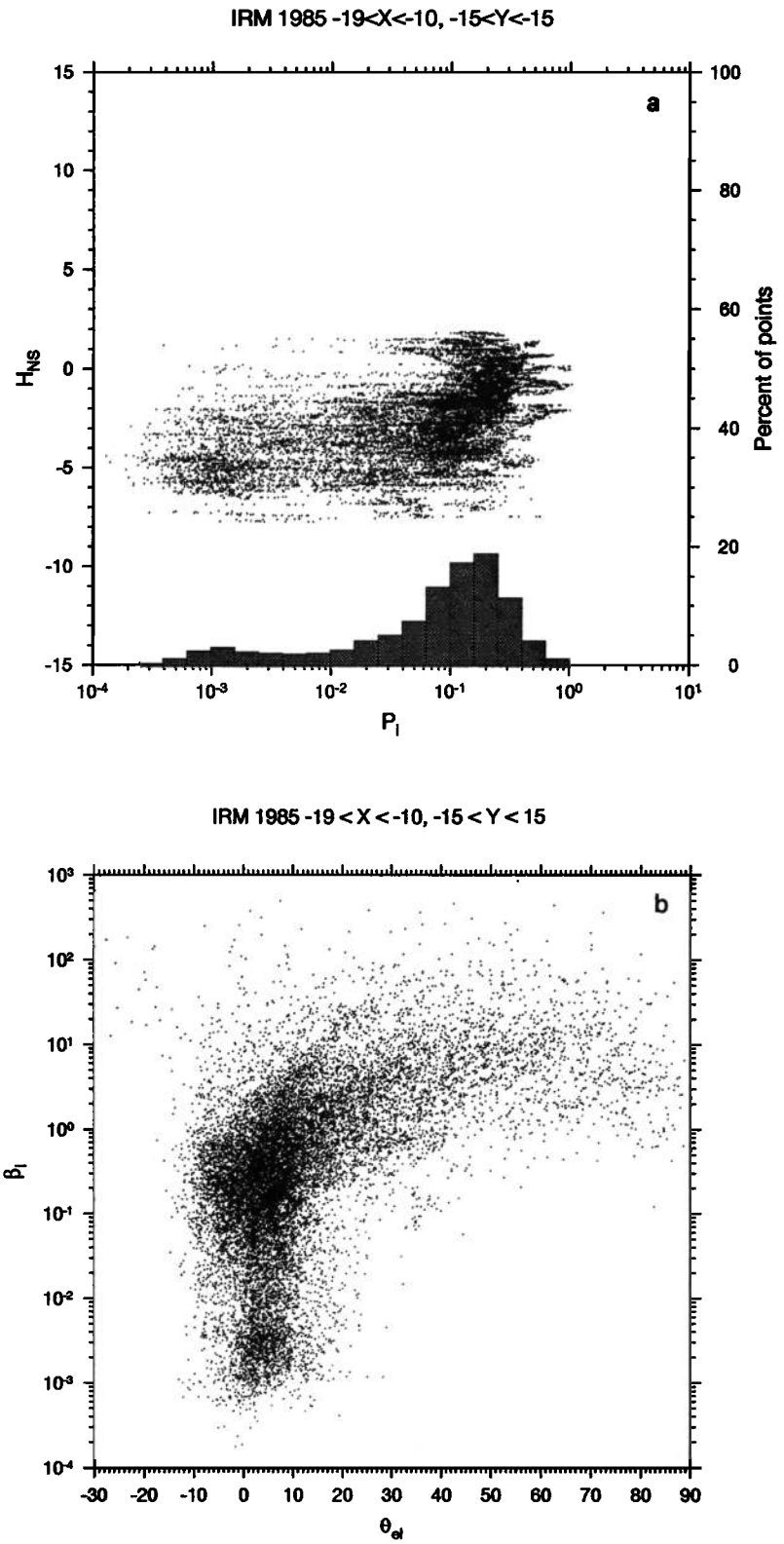

Figure 1. (a) Scatterplot of the AMPTE/IRM data at 5-s resolution and factor 10 decimation (i.e., plotting every tenth sample) in H_{NS}-P_i space. P_i (nPa) is the ion thermal pressure and H_{NS} (R_E) is the distance from the *Hammond et al.* [1994] neutral sheet model. Two clusters of points appear: a high pressure, low H_{NS} cluster, of presumably plasma sheet data, and a low pressure, high H_{NS} cluster of presumably lobe data. A P_i histogram (scale is presented on the right vertical axis) shows a minimum at ~0.5 x 10^{-2} nPa. Based on this scatterplot and its ISEE 2 counterpart (Figure 2a) we defined as non lobe samples those that have $P_i > 0.01$ nPa. (b) Scatterplot of the IRM data in β_i-θ_{el} space; θ_{el} (degrees) is the elevation angle of the magnetic field vector above the GSM equatorial plane; β_i is the ratio of the ion thermal pressure to the magnetic pressure.

the distribution of samples in a θ_{el}-β_i space can be instructive regarding the different plasma regimes of the plasma sheet. Figures 1(b) and 2(b) show such scatterplots for the IRM and ISEE 2 data respectively, after a factor 10 decimation. Lobe samples were included in these scatterplots; they can be seen as a cluster of points at the lowest β_i values. The range of elevations for the lobe samples is approximately between -10° and 20° in both data sets.

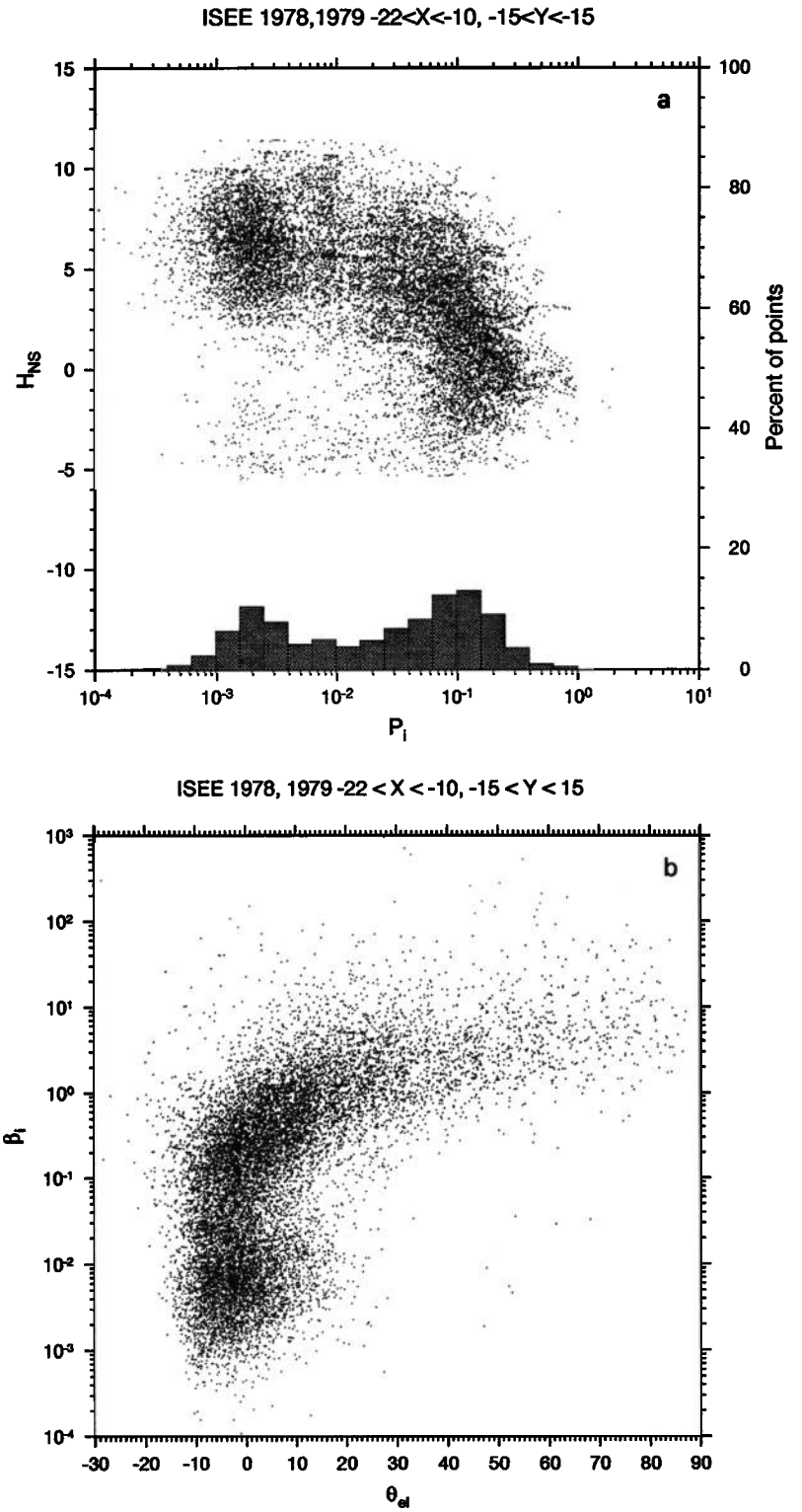

Figure 2. (a) Same as in Figure 1 (a) but for the ISEE 2 data set (12 s resolution, factor 10 decimation). A minimum in the distribution at ~10^{-2} nPa signifies a change from lobe to plasma sheet samples. (b) Same as in Figure l(b) but for the ISEE 2 data set. The similarity of this scatterplot with the one of Figure 1(b) justifies the use of the same criteria to separate IPS from OPS in both the IRM and ISEE 2 data sets.

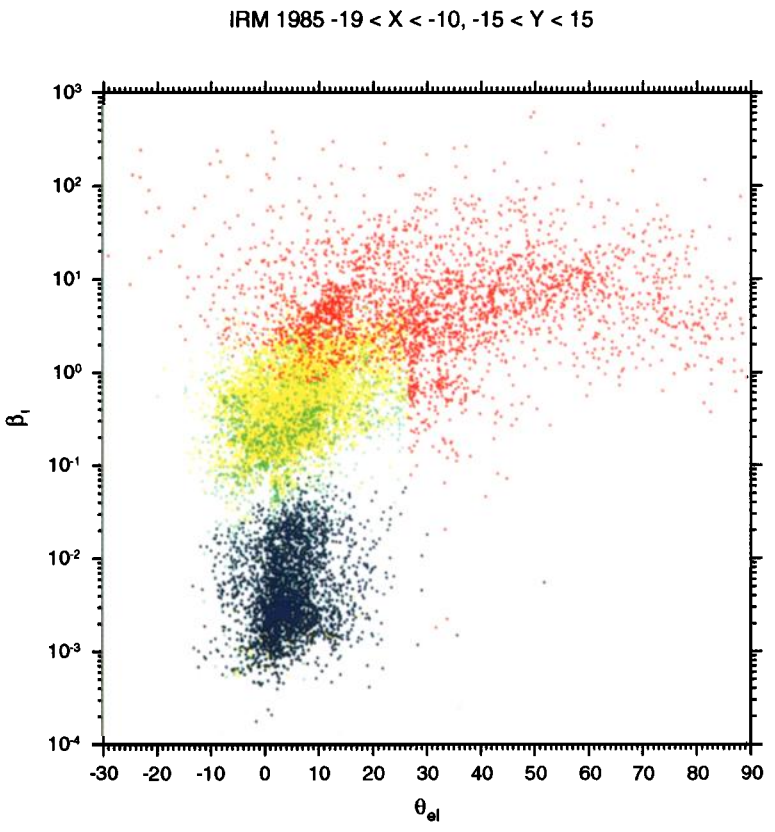

Plate 1. Same as in Figure 1b except that the ICPS, OCPS, PSBL defined by *Baumjohann et al.* [1990] are now shown in red, yellow and green, respectively. Blue denotes lobe samples, as identified by our criteria. There is a continuum of states between high β_i, high θ_{el} points (presumably closer to the neutral sheet) and low β_i, low θ_{el} points closer to the lobe. In particular there is no clear separation between OCPS and PSBL in this space. We defined two regions based on, β_i after excluding lobe samples: A region of $\beta_i > 0.5$ that incorporates the ICPS, which we termed inner plasma sheet (IPS) and a region of $\beta_i < 0.5$ which incorporates much of the PSBL as defined by *Baumjohann et al.* [1990].

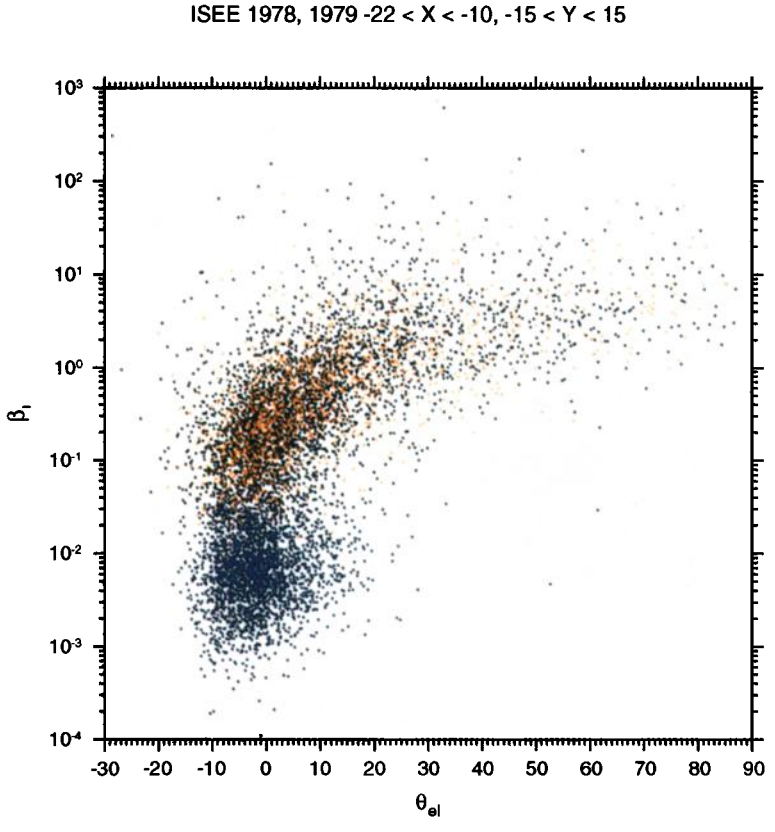

Plate 2. Same as in Figure 2b except that the CPS and PSBL defined by *Huang and Frank* [1986] are shown in black and orange, respectively. Blue denotes lobe samples, as identified by our criteria (see text).

It is noteworthy that in Figures 1(b) and 2(b) there is no clear separation of different plasma regimes between the high elevation, high β_i samples and the low elevation, low β_i samples. Instead, there seems to be a continuity of states between these two plasma conditions. At best, we can identify a high beta region incorporating most of the high elevation samples, and a low beta region of smaller, lobelike elevation. We chose $\beta_i = 0.5$ as the dividing line between the two regions compromising between the need to have a large enough data set and our goal to study flows as close to the neutral sheet as possible. Our choice of β_i as an indicator of plasma sheet distance is based on two reasons: First, the quantity β_i is one that varies most dramatically across the plasma sheet according to *Baumjohann et al.* [1989, Figure 3]. Second, if we assume for simplicity a Harris sheet model for the plasma sheet [*Harris*, 1962] we can express β_i as a monotonic function of the distance to the neutral sheet divided by the current sheet scale length. A constant β_i value under different solar wind conditions or downtail distances simply reflects a constant distance from the neutral sheet scaled by the current sheet thickness.

We termed the plasma regime with $\beta_i > 0.5$ the inner plasma sheet (IPS) and the regime with $\beta_i < 0.5$ the outer plasma sheet (OPS). Our terminology distinguishes the regions defined here from the terms PSBL, CPS, OCPS, ICPS defined by other authors [*Huang and Frank*, 1986; *Baumjohann et al.*, 1990].

To visualize the relationship of our IPS and OPS regions to the plasma sheet regions defined by other authors, we present previously defined regions in color, in Plates 1 and 2. Lobe samples defined in the previous paragraph are plotted in blue in both figures. Plate 1 presents in red, yellow, and green the samples of the AMPTE/IRM database that would have been defined as ICPS, OCPS and PSBL, respectively, using the *Baumjohann et al.* [1990] criteria. Our definition of IPS ($\beta_i > 0.5$) includes most of the ICPS samples and some OCPS samples. The OPS ($\beta_i < 0.5$) includes most of the PSBL samples and some OCPS samples. Plate 2 presents, in black and orange, the samples from the ISEE 2 database that would have been defined as CPS and PSBL respectively, based on the *Huang and Frank* [1986, 1987] criteria (described in the introduction). We used 12-s resolution data, although *Huang and Frank* [1986, 1987] defined their regions based on 2- to 8-min resolution data. The definitions of CPS and PSBL do not represent different plasma regimes in θ_{el}-β_i space, even when applied to high resolution data, and thus bear no apparent relationship to our definition of IPS and OPS. The use of the distance from a model neutral sheet in the definition of plasma sheet regimes may be the reason why the *Huang and Frank* [1986, 1987] criteria are not commensurate with our IPS and OPS plasma sheet separation [*Cattell and Elphic*, 1987].

The similarity of the behavior of the IRM and ISEE 2 databases in the θ_{el}-β_i space gives us confidence that the criteria we have developed are satellite-independent, and may provide a meaningful approach of identifying the innermost from the outermost plasma sheet layers. Our identification of two plasma sheet regions interpreted as plasma domains at different distances from the neutral sheet agrees with the sense of distance from the neutral sheet implied by the *Baumjohann et al.* [1990] criteria of three plasma sheet regions. This ensures that the definition of BBFs used in this paper will be compatible with the one used in our earlier papers [*Angelopoulos et al.*, 1992a, 1992b]. Our criteria also avoid the problem of a "circular argument" in the investigation of the statistical correlation between BBFs and dipolarization. Finally, our criteria avoid the use of the electron measurements to identify plasma sheet regions. We must note at this point that a significant portion of the original AMPTE/IRM database lacks simultaneous measurements of the electron density even if the ion moments and magnetic field measurements are present. That portion of the database was not used in the plasma sheet studies of *Baumjohann et al.* [1989, 1990] but has been kept in our analysis, giving us a statistical ensemble that would otherwise have been 42% smaller.

After extracting the lobe samples from our databases we plotted the spatial coverage of the plasma sheet samples in Plates 3 and 4 for the AMPTE/IRM and ISEE 2 data sets respectively in the X-Y (top panels) and the Y-H_{NS} (bottom panels) planes. (Coordinates are in the AGSM system.) The orbital bias toward the dusk sector on the X-Y plane in the IRM data set is obvious, as is the more uniform plasma sheet coverage by the ISEE 2 satellite. Note in the Y-H_{NS} projection of the plasma sheet data, that IRM samples the plasma sheet closest to the expected position of the neutral sheet most often at premidnight, whereas ISEE 2 is most often closest to the statistically expected neutral sheet position at midnight and postmidnight.

4. Case Studies of BBF Events

We defined BBFs to be segments of continuous ion flow magnitude V_i above 100 km/s in the plasma sheet, during which V_i exceeds 400 km/s for at least one sample period in the IPS. Samples of $V_i > 400$ km/s that were less than 10 minutes apart were considered to belong to the same BBF event, even if the velocity dropped below 100 km/s between these samples. BBFs were thus defined in a way similar to our earlier papers [*Angelopoulos et al.*, 1992a, 1992b], but for the use of the IPS in lieu of the ICPS as the region where the fast flows had to reside to qualify a flow event as a BBF event. There were 114 BBFs in the AMPTE/IRM database and 241 BBFs in the ISEE 2 database. Only 22% (29%) of the BBF samples belong to the OPS in the AMPTE/IRM (ISEE 2) database.

In the following we present a few cases of BBFs from the ISEE 2 and IRM databases in order to demonstrate the applicability of the region identification, the pertinence of the BBF selection criteria and the need to study BBFs irrespective of geomagnetic activity. In no case study or statistical analysis in this paper did we use any criterion other than the one described in the previous paragraph to classify a fast flow occurrence as a BBF event and to define BBF boundaries. Similarly, only the region identification criteria of Section 3 were used to determine the magnetotail region the spacecraft was in. All references to other quantities (field orientation and magnitude, plasma density and temperature) and the associations of those quantities with certain tail plasma regions are made only to justify the computer-automated application of the BBF selection and region identification criteria.

4.1. An ISEE 2 BBF Study

The magnetotail crossing presented in this section encompasses fast flows with both tailward and earthward V_x. This ISEE 2 near-neutral sheet tailward flow case study is the first one described in terms of BBFs. Since previous analyses of BBFs were carried out based on the AMPTE/IRM data set which is dominated by earthward BBFs, tailward BBFs will be segregated in our analysis in recognition of the possibility that they may not have similar characteristics to earthward ones.

On April 3, 1979, at 0100 UT, ISEE 2 was in the magnetotail, very close to the X-Y AGSM plane, 20 R_E downtail and close to local midnight. Figure 3 shows the plasma and magnetic field observations for a 3-hour interval starting at 0100 UT. The AE

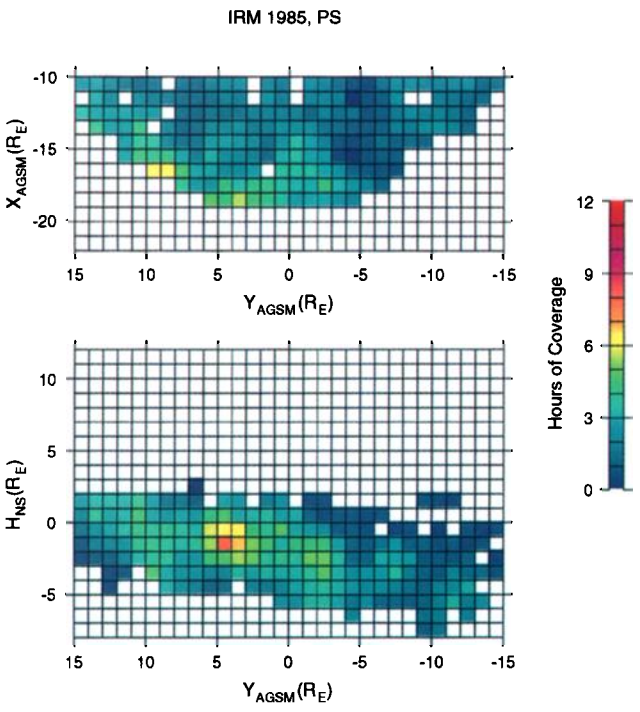

Plate 3. AMPTE/IRM coverage in hours, on the X-Y and Y-H_{NS} planes (X and Y are in aberrated GSM coordinates). Nearest neighbor smoothing was applied to the data in each 1 x 1 R_E^2 bin.

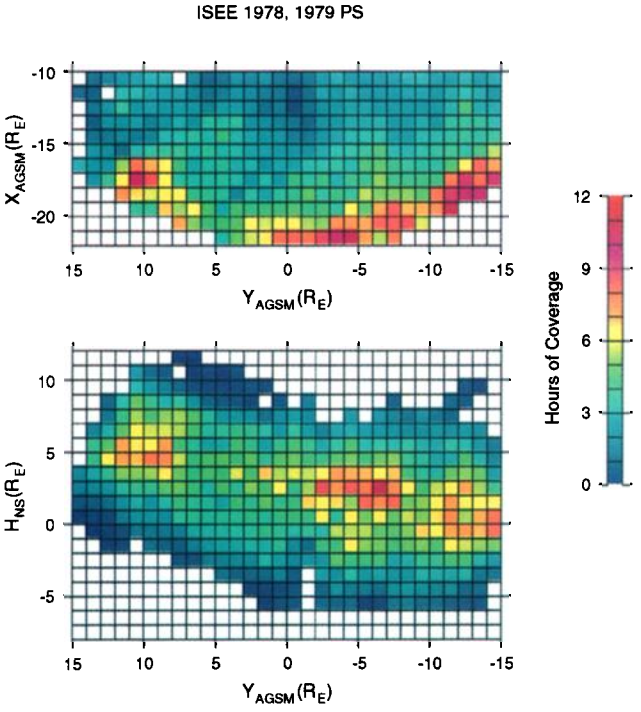

Plate 4. Same as in Plate 3, but for the ISEE 2 satellite.

index, plotted on the top panel, shows that there was moderate geomagnetic activity during this period (100 < AE < 500 nT). The magnetotail regions are denoted in the horizontal bar above the AE trace by different colors: Black denotes IPS, gray denotes OPS, and white denotes lobe. Three BBF events were identified in this interval; they are highlighted by the gray vertical shading.

Prior to the first large tailward flow event (0128 UT) the spacecraft traversed regions of zero B_x, indicating that it was very close to the neutral sheet. The plasma temperature was 7-8 keV and the density was 0.10 - 0.15 cm^{-3}. Upon onset of the tailward flows B_x remained low, and a second neutral sheet encounter was observed at 0135 UT, very close to the peak of the tailward flow event. During the first part of the tailward flow event (0128-0141 UT) the ion temperature decreased but the ion density remained fairly constant and the spacecraft remained in the IPS. During the 0135 UT neutral sheet encounter (peak of tailward flow) the ion temperature had reduced down to 5-6 keV but the ion density was 0.14 cm^{-3}, roughly similar to the pre-BBF conditions.

After the peak tailward flow, the spacecraft started encountering regions of stronger field, and lower density and temperature, indicating that it was exiting toward the lobe. However, the ion temperature remained at the 1-2 keV level and the ion density did not subside below 4 x 10^{-2}, indicating that the spacecraft did not fully exit to the lobe. According to our region definition, when the magnetic field started to increase the spacecraft entered the OPS and did not exit to the lobe, in agreement with the impression gained by a visual inspection of the data.

The second BBF event of this study has large earthward and tailward flows within it, the earthward flows being accompanied by B_z increases (possible dipolarizations). However, the flow magnitude does not subside below 400 km/s for more than 10 minutes between the earthward and tailward bursts, and thus our criterion incorporates both kinds of fast flows in the same BBF event. On the basis of the positive average value of V_x this particular event can be characterized as earthward. However, it could also be considered as "mixed" based on the existence of both earthward and tailward fast flows (V_i > 400 km/s and V_x both positive and negative) within its temporal boundaries.

Several minutes after the second BBF event the spacecraft measured high speed flows in a fairly strong and taillike field region. These high speed flows are classified as OPS high speed flows. Our computer-automated BBF selection excludes these OPS high speed flows from the profile of the second BBF event because low flow (V_i<100 km/s) samples intervene between the second BBF event and the fast OPS flows, thus marking the end of that BBF event. Such OPS flows could conceivably map to equatorial activations further downtail from the satellite and will not be considered in this paper.

The onset of the third BBF event occurred in a plasma sheet region of low density, low temperature and strong magnetic field, suggesting that the spacecraft was far from the center of the current sheet. The region is classified as OPS in accordance with the impression gained from the time series of the measurements. Later during the evolution of the event the magnetic field magnitude decreased, its Z component increased and the ion temperature also increased. The spacecraft then entered the IPS. The existence of high speed flows in the IPS permits this high speed flow sequence to be classified as a BBF event, even if it starts in the OPS.

During and after the subsidence of the earthward high speed flows, the field became more dipolar and the plasma got hotter, as noted for BBFs in the AMPTE/IRM database [*Angelopoulos et al.*, 1992a, 1992b]. Furthermore, the ion density decreased from 0.1 - 0.15 cm^{-3} prior to the onset of the earthward BBFs to 0.5 - 0.1 cm^{-3} (i.e., by a factor of 2) during and after the BBF events. This is in agreement with the observations of *Baumjohann et al.* [1990] that high speed flows tend to coincide with low ion densities (their

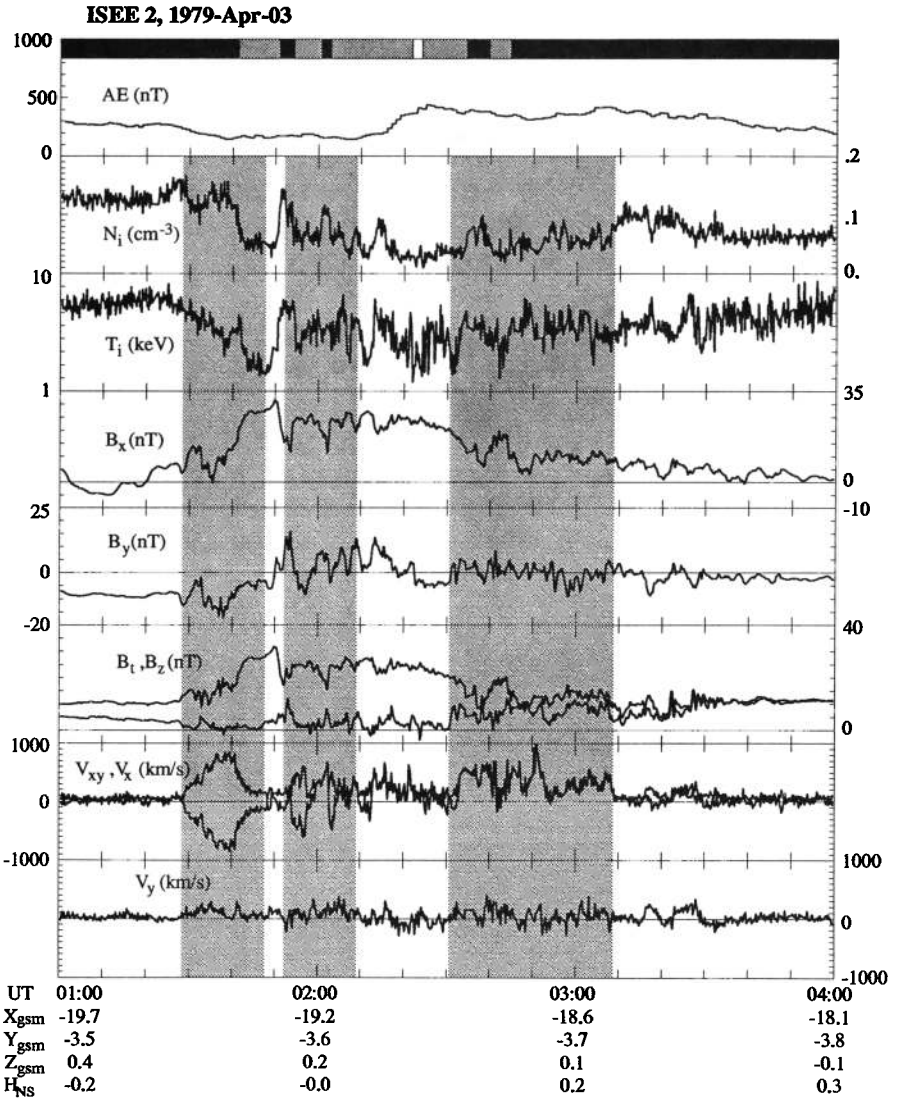

Figure 3. A magnetotail crossing encompassing three BBF events during moderately active conditions. The top panel shows the AE index at 1-min resolution. The rest of the panels are at 12-s resolution. Shown from top to bottom are the ion density N_i; the ion temperature T_i; the X and Y GSM components of the magnetic field; the Z GSM magnetic field component along with the field magnitude B_t; the X and Y components of the ion velocity in spacecraft coordinates (very close to GSE) along with the magnitude of the XY component $V_{xy} = (V^2_x+V^2_y)^{1/2}$. Universal time is given at the bottom, as well as the spacecraft location GSM coordinates and the distance from the *Hammond et al.* [1994] neutral sheet location H_{NS}. The vertical shaded regions denote the BBF events identified based on the criteria explained in section 3. The horizontal bar code above the AE index trace denotes magnetotail regions according to the criteria detailed in Section 2.

Figure 4). Such a correlation was not evident in the superposed epoch analysis on flow bursts by *Angelopoulos et al.* [1992]. It is possible that the density decrease is a property of the plasma conditions surrounding BBF events but not of the individual flow bursts within BBFs.

For the purposes of this paper we divided the BBFs into earthward $(\overline{V}_x > 0)$ and tailward $(\overline{V}_x < 0)$ according to the average value of V_x during each BBF event. The first BBF event in our case study is tailward and is accompanied by ion cooling, and no signature of dipolarization. Most of the 47 tailward BBFs that can be found in the ISEE 2 database and are not suffering from spatio-temporal ambiguities (i.e., the spacecraft remains within the plasma sheet during and after the event) have similar signatures. Frequently, the magnetic field turns southward for limited periods during tailward BBFs. The ISEE 2 tailward BBF case study that was presented here, however, does not exhibit that B_z behavior. An extended statistical analysis of the evolution of the plasma and magnetic field during such events is beyond the scope of this paper. Here we will limit ourselves to an investigation of the spatial dependence of tailward BBFs and their correlation with B_z.

4.2. An AMPTE/IRM BBF Study

Bursty bulk flow events from the AMPTE/IRM database have been presented elsewhere [*Angelopoulos et al.*, 1992a, 1992b] in

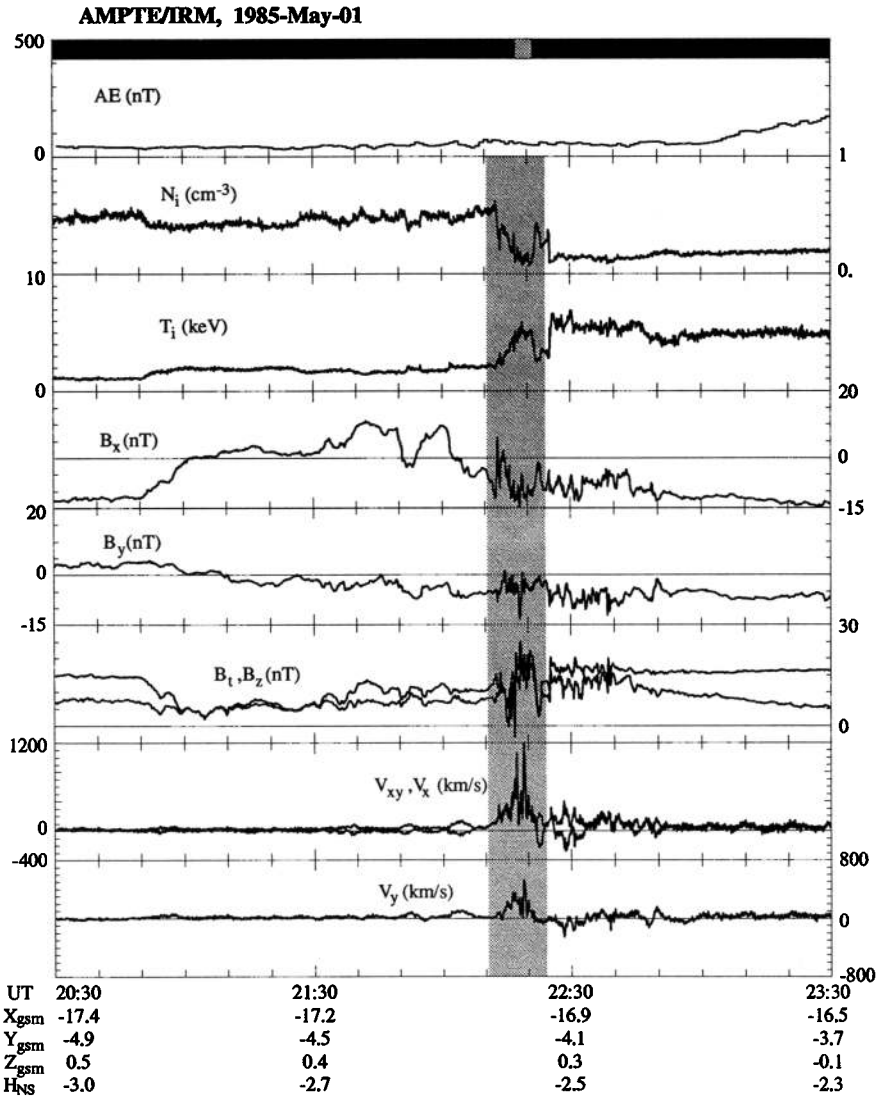

Figure 4. A magnetotail crossing encompassing a BBF event during geomagnetically quiet conditions. The top panel shows the AE index at 1-min resolution. The rest of the panels are at 5-s resolution. The quantities plotted are the same as in Figure 3, but for the ion velocity whose components are plotted here in GSM coordinates and its magnitude V_i is computed from a three-dimensional velocity vector $V_i = (V^2_x+V^2_y+v^2_z)^{1/2}$.

detail. With this example we will focus on the plasma sheet identification criteria and the similarities between ISEE 2 and AMPTE/IRM BBFs.

On May 1, 1985 at 2030-2330 UT the AMPTE/IRM satellite was on an inbound orbit in the near midnight sector approximately 17 R_E downtail. Figure 4 shows the plasma and magnetic field data from this interval in the same format as Figure 3. As evidenced by the sign changes of B_x, the satellite encountered the neutral sheet several times prior to 2210 UT, the approximate time that the ion flow started to assume very large values. The shaded interval represents our computer-automated definition of a BBF event at that time. Several encounters (approximately at 2213 and 2215 UT) of the neutral sheet took place during the BBF event as well. The Z component of the magnetic field was the dominant component during this interval.

During the BBF event the ion density decreased and the ion temperature increased. The post-BBF plasma sheet was hotter and less dense than the pre-BBF plasma sheet. The plasma sheet magnetic field exhibited strong dipolarization; the strong dipolar component remained present for more than half an hour after the event. These characteristics are similar to the characteristics of the earthward BBF event described earlier based on ISEE 2 data.

Most of the BBF events from both the AMPTE/IRM and the ISEE 2 databases took place under geomagnetically active conditions (AE>100 nT). However, some events (like the one of Figure 4) did take place during geomagnetically quiet intervals as determined by the AE index, casting doubt on the ability of AE to qualify the instantaneous transport conditions at a given position in the plasma sheet. In addition, as detailed in this case study, geomagnetically quiet time BBFs exhibit characteristics similar to the active time ones. It is for these reasons that we abandoned the use of AE as a part of the definition of the BBF activity and attempted to characterize magnetotail transport, at least initially, irrespective of the AE index.

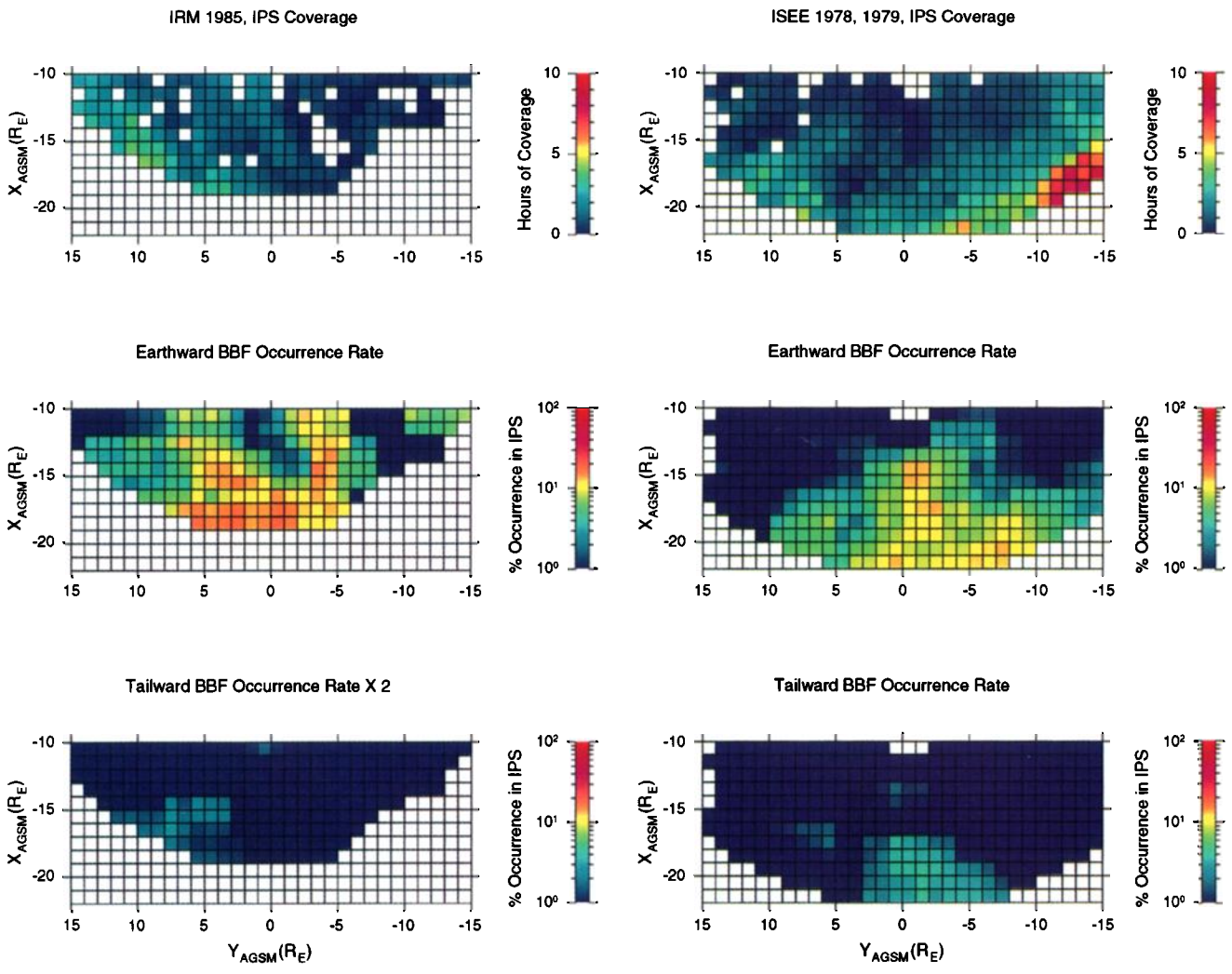

Plate 5. Top: IRM coverage of the inner plasma sheet (IPS). Nearest neighbor smoothing was applied to the 1 x 1 R_E^2 bins. Middle: The occurrence rate of earthward BBFs in the IPS. Data were running averaged with a 3 x 5 R_E^2 sliding window on the X-Y AGSM plane, centered on 1 x 1 R_E^2 bins within the coverage area of the orbit. Bottom: Occurrence rate of tailward BBFs (multiplied by two) in the same format as middle panel.

Plate 6. Same as in Plate 5 but for the ISEE 2 satellite, and without rescaling of the tailward BBF occurrence rate.

5. Spatial Dependence of BBFs

Plates 5 and 6 show the spatial dependence of the occurrence rate of earthward BBFs $\left(\overline{V}_x > 0\right)$ in the IPS (middle panels), and the IPS coverage on which the occurrence rates were based (top panels), from the IRM and ISEE 2 databases respectively. A 3 x 5 R_E^2 sliding area centered on 1 x 1 R_E^2 bins within the limits of the satellite coverage was used for the calculation of the occurrence rates. The satellite coverage in the IPS was subjected only to nearest neighbor smoothing. In both data sets the earthward BBFs comprise 10-15% of the time spent by the spacecraft at apogee and close to midnight, although earthward BBFs in the IRM data set are ~50% more frequent than the ones in the ISEE 2 data set.

The spatial dependence of the earthward BBF occurrence rate on both satellites is roughly similar to the one of high speed flows in the plasma sheet described by *Baumjohann et al.* [1990] for the IRM data set, i.e., it tends to increase with distance from Earth and proximity to midnight. In particular, our results from the ISEE 2 data set (which does not suffer from limited coverage in the postmidnight IPS as does the IRM data set) indicate that indeed the occurrence rate of BBFs decreases with distance away from midnight in the postmidnight sector as well as in the premidnight sector. It is noteworthy, however, that the increase of earthward BBF occurrence rate with distance from Earth does not seem to continue downtail of X = -19 R_E in the ISEE 2 data set.

The bottom panels of Plates 5 and 6 show the spatial dependence of the occurrence rate of tailward BBFs $\left(\overline{V}_x < 0\right)$ in the IPS. In agreement with the results of *Baumjohann et al.* [1989], there are very few tailward BBFs in the IRM data set (notice that we had to multiply the occurrence rate of tailward BBFs on IRM by 2 to render them visible on our color-scale). The occurrence rate of tailward BBFs is also small in the ISEE 2 data set earthward of X = -19 R_E. Overall, however, there are clearly more tailward BBFs in the ISEE 2 database than in the IRM database; their occurrence rate increases with distance from Earth and proximity to midnight. It is noteworthy that the region where the (few) tailward BBFs are observed on IRM is the region where the satellite coverage is closest to the expected position of the neutral sheet (Plate 3). The same argument applies for the ISEE 2

satellite, which is more often closest to the expected neutral sheet position at postmidnight (also see Plate 4). Thus, the local time distribution of the tailward BBFs is consistent with a thin plasma sheet during tailward flow conditions [*Hones and Schindler*, 1979, and references therein].

It is expected from the studies of *Baumjohann et al.* [1989, 1990], which revealed a positive correlation between fast flows and AE, that the occurrence rate of BBFs should also increase with increasing geomagnetic activity. The dependence of the BBF occurrence rates on geomagnetic activity has not been incorporated in Plates 5 and 6; these plates include data from all activity levels. For this reason we now attempt to investigate the quantitative differences of the total (sum of earthward and tailward) BBF occurrence rate between the two satellites as well as between different distances for the same satellite, taking the geomagnetic activity into account. Figure 5 shows the results of this investigation. The data from each data set in the spatial region of interest were divided into four quartiles based on AE. We found the occurrence rate of BBFs in every AE quartile and we assigned it to the average value of AE in the quartile. The region of IRM and ISEE 2 spatial overlap i.e., $-15 > X > -19$ R_E, $|Y| < 5$ R_E, where both satellites have a fairly good coverage of the IPS is a particularly interesting region for an intersatellite comparison. In addition, the region $X < -19$ R_E, $|Y| < 5$ R_E can be studied in comparison with the "overlap region" to explore the X dependence of the ISEE 2 BBF occurrence rate.

Figure 5 shows that the occurrence rates of ISEE 2 and IRM BBFs in the region of overlap are different at large values of AE (AE > 100 nT): BBFs are 50% more frequent in the IRM database than in the ISEE 2 database. It is not clear what the origin of this difference is. A possible explanation may be the following: If the plasma sheet thickness were to remain constant during BBFs, a simple division of the cumulative BBF duration by the satellite's time in the IPS would give us the occurrence frequency of BBFs. However, if BBFs are associated with plasma sheet reconfigurations, they may be responsible for observing (or missing) a BBF event. If the two data sets had the same average distance from the neutral sheet then they would experience similar effects in the occurrence rate of BBFs due to the possible plasma sheet reconfigurations. However, the IRM satellite is, on average, closer to the nominal position of the neutral sheet relative to the ISEE 2 satellite (Plates 3 and 4). It is conceivable that this orbital bias coupled with possible plasma sheet reconfigurations during BBFs cannot be normalized away by a simple division of the cumulative BBF duration by the number of samples in the IPS.

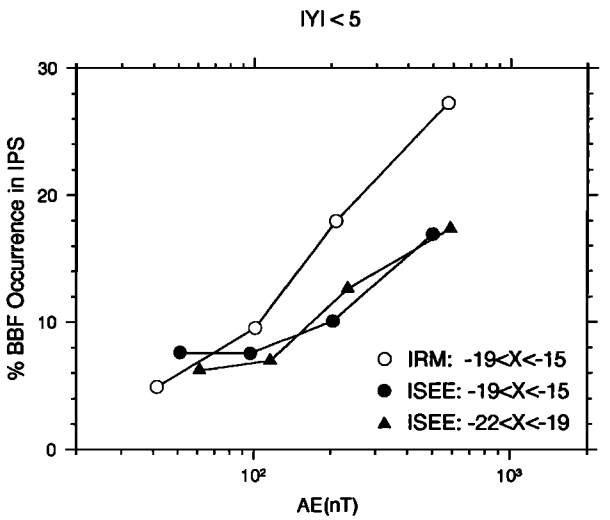

Figure 5. Dependence of the occurrence rate of center-tail BBFs (earthward and tailward) on activity. The ISEE 2 data were further segregated into two categories, sunward and tailward of $X = -19$ R_E. For each data set and category the data were divided into four quartiles based on AE and the % BBF occurrence rate was calculated in each quartile and plotted against the average AE value for the quartile.

In addition, the occurrence rate of the sum of earthward and tailward BBFs, tailward of $X = -19$ R_E does not seem to follow the increasing trend with distance from Earth, seen earthward of that value. This suggests that the occurrence rate of BBFs stabilizes at that distance, although it is not clear whether the orbital characteristics of the ISEE 2 mission are responsible for this observation: As the average distance of ISEE 2 from the expected neutral sheet position increases tailward of 19 R_E, it is possible (as noted in the previous paragraph) that a simple division with the number of samples in the IPS may not be a sufficient normalization of the observed duration of BBFs. An analysis of other data sets capable of probing regions tailward of 22 R_E with a common methodology is necessary to determine the validity of this conjecture.

In both data sets BBFs are observed with a small but finite occurrence rate (~6%) even under low AE conditions. This is in agreement with the earlier observations by *Baumjohann et al.* [1989] on the occurrence rates of fast flows in the plasma sheet as well as with Cattell and Mozer's [1984] observation that 10 out of their 74 events did not occur within 30 minutes from any peak in AE greater than 100 nT. At very active times the BBF occurrence rates can be as large as 15-20% or 25-30% in the ISEE 2 and IRM data sets, respectively.

The above results quantify the frequency of BBFs, their spatial distribution and their statistical dependence on geomagnetic activity. Our observations also pinpoint the existence of an important subset of BBFs, namely tailward ones, that essentially exist only in the ISEE 2 data set predominantly tailward of ~19 R_E and are very infrequent in the IRM data set mostly due to its smaller apogee.

5.1. More on Tailward BBFs

Even in the region of spatial overlap ($-15 > X > -19$ R_E, $|Y| < 5$ R_E) there are more tailward BBFs on ISEE 2 than on IRM. Aside from possible differences in instrument response a major difference between the data sets in the region of overlap is the solar epoch: ISEE 2 was traversing the magnetosphere just prior to solar maximum and IRM near solar minimum. It is conceivable that a near-Earth neutral line forms close to Earth more frequently during solar maximum conditions and less frequently during solar minimum conditions due to the different geomagnetic activity under such conditions. Table 1 shows the median AE, the number of BBFs and the ratio of durations of tailward BBFs to all BBFs in each spatial region specified. The information in Table 1 confirms that the IRM data from the region of spatial overlap were acquired during geomagnetically quieter conditions than the ISEE 2 data from the same region, and thus provides a possible explanation for the scarcity of tailward BBF observations in IRM.

Table 1 also shows that the percent duration of tailward BBFs relative to all BBFs increases from 15% earthward of $X = -19$ R_E to 23% tailward of that distance, an increase that cannot be attributed to an increase in geomagnetic activity since the median AE is actually lower in the latter subset. We also included in the

Table 1. Tailward BBFs and Geomagnetic Activity

Spacecraft	Region (|Y| < 5), [R_E]	Median AE in IPS [nT]	Number of BBF Events: Tailward	Number of BBF Events: All	Percent BBF duration: Tailward/All	Number of samples: $\|V_i\|$ > 400 km/s, Tailward, B_z<0	Number of samples: $\|V_i\|$ > 400 km/s, Tailward, All	Number of samples: $\|V_i\|$ > 400 km/s, All	Number of samples: Tailward/All
	-19 < X < -15	134	3	46	3 (7)†	4	53	1040	5%
ISEE 2	-19 < X < -15	187	7	42	15 (13)	11	30	426	7%
ISEE 2	X < -19	156	15	64	23 (18)	109	205	568	36%

† Percentages in parentheses refer to |Y| < 10 R_E.

same table the percent duration of tailward over all BBFs in the region |Y| <10 R_E. That region was used by *Hayakawa et al.* [1982] to select midnight passes of the IMP 6 satellite and is the location of predominant occurrence of fast flows in the *Nakamura et al.* [1994] study of the IMP 6, 7, and 8 satellite data. The relative frequency of tailward versus all BBFs increases from 13% earthward of X=-19 R_E to 18% tailward of that distance in the ISEE 2 data set. These numbers compare favorably with the figure of 22% of the *Hayakawa et al.* [1982] study (20 out of 90 of their fast flow events were tailward) and the figure of 26% of the *Nakamura et al.* [1994] study (24 out of 92 fast flow events were tailward). Assuming that local time orbital biases of the data sets and event identification methodology do not severely affect a comparison between the different data sets, the above results suggest that tailward BBFs become an increasingly more substantial fraction of all BBFs with increasing distance from Earth, as far downtail as X ≈ -30 R_E.

Tables 2, 3, and 4 provide lists of the tailward BBFs that were observed in the three subsets that appear in Table 1. Also shown in the above tables are the average velocity during each BBF event, the average value of B_z and the average value of $E_y = V_x B_z$ in kV/R_E. A northward B_z is not unexpected during fast tailward flows generated by reconnection in some occasions (e.g., plasmoids) but it is followed by southward B_z. A southward average B_z and a positive average E_y is expected if open lobe flux has been reconnected in the near-Earth neutral line picture. It is noteworthy that in all regions most tailward BBFs are associated with northward average B_z and a negative average E_y, thus corresponding to tailward transport of closed magnetic flux. These BBFs do not conform to the conventional lobe reconnection picture without the addition of significant complication and deserve further attention. The three tailward IRM BBFs and most of the ISEE 2 BBFs observed in the region of spatial overlap belong to this category. Interestingly, however, the number of tailward BBF events that do comply with a positive average E_y picture expected during lobe reconnection increases with distance from Earth (1 out of 7 in Table 3, but 4 out of 15 in Table 4). Comparison of these results with the findings of *Hayakawa et al.* [1982] and *Nakamura et al.* [1994] that 70-75% of all tailward fast flow events are associated with a southward average B_z at X = -25 to -30 R_E suggests that the tailward BBFs may organize according to the near-Earth reconnection picture only further downtail from the region where they are generated.

Table 2. AMPTE/IRM Tailward BBFs in Region -19 < X < -15 R_E, |Y| < 5 R_E

Begin Time, UT	Δt, s	X_{AGSM}, R_E	Y_{AGSM}, R_E	H_{NS}, R_E	V_X, km/s	V_Y, km/s	B_Z, nT	E_Y, kV/R_E
April 10, 1985 2024:05	305	-15.0	3.2	-1.7	-48.	177.	5.	-2.3
April 24, 1985 0602:30	350	-18.5	3.4	-1.3	-105.	-16.	7.	-1.7
April 29, 1985 1932:30	505	-18.2	4.8	-2.7	-5.	123.	3.	-0.7

Table 3. ISEE 2 Tailward BBFs in Region -19 < X < -15 R_E, |Y| < 5 R_E

Begin Time, UT	Δt, s	X_{AGSM}, R_E	Y_{AGSM}, R_E	H_{NS}, R_E	V_X, km/s	V_Y, km/s	B_Z, nT	E_Y, kV/R_E
April 3, 1979 0153:42	972	-18.9	-4.9	0.0	-2.	106.	3.	1.3
April 5, 1979 1250:19	240	-18.3	-4.2	-1.1	-251.	-181.	14.	-28.
April 15, 1979 0148:55	552	-18.9	-1.6	0.8	-114.	112.	-5.	5.
April 15, 1979 0201 :07	624	-18.8	-1.6	0.8	-94.	162.	-3.	3.
April 15, 1979 0215:19	936	-18.6	-1.6	0.8	-38.	149.	1.	0.
April 22, 1979 0646:07	864	-18.4	0.7	1.2	-35.	211.	0.	1.
April 24, 1979 1530:59	438	-18.8	1.6	-1.3	-143.	108.	7.	-6.

Table 4. ISEE 2 Tailward BBFs in Region $X < -19\ R_E$, $|Y| < 5\ R_E$

Begin Time, UT	Δt, s	X_{AGSM}, R_E	Y_{AGSM}, R_E	H_{NS}, R_E	V_X, km/s	V_Y, km/s	B_Z, nT	E_Y, kV/R_E
March 28, 1979 1631:28	444	-21.7	-4.4	1.1	-366.	-96.	-7.4	20.9
April 2, 1979 1116:28	804	-21.8	-1.9	3.2	-252.	62.	-1.5	0.2
April 2, 1979 1616:53	1104	-21.8	-3.6	0.3	-25.	241.	1.7	-0.2
April 2, 1979 1644:17	480	-21.7	-3.8	0.1	-223.	78.	0.8	0.8
April 2, 1979 1816:05	240	-21.5	-4.1	-0.5	-218.	-39.	-3.3	8.0
April 2, 1979 2134:41	1368	-20.7	-4.6	-0.8	-242.	-9.	0.2	1.6
April 3, 1979 0129:06	1164	-19.1	-4.9	-0.1	-400.	90.	1.4	-3.1
April 5, 1979 0750:07	192	-20.4	-3.5	2.0	-225.	-37.	15.1	-23.7
April 12, 1979 1435:46	708	-19.8	-1.7	-1.1	-239.	20.	-0.3	0.5
April 14, 1979 1543:42	1896	-21.8	0.5	1.0	-133.	164.	0.0	1.4
April 14, 1979 1653:06	492	-21.7	0.1	0.7	-49.	172.	0.4	-0.1
April 17, 1979 0817:54	720	-20.2	0.3	1.7	-143.	112.	3.7	-3.1
April 17, 1979 1026:54	804	-19.2	-0.2	0.2	-220.	197.	0.4	1.1
April 21, 1979 1441:54	336	-21.1	4.5	2.7	-12.3	148.	6.1	-0.1
April 24, 1979 1111:46	324	-20.3	3.2	0.8	-190.	58.	0.7	-0.9

5.2. Statistics of BBF Flow Samples

It is instructive to investigate the angular distribution of the flow samples within BBF events and the evolution of that distribution from one spatial region to another. This is shown in Figure 6 for the same spatial regions as those of Table 1 (also see figure caption). Different subsets are in different rows. The angular distribution of the BBF flow samples' occurrence rates is shown in the left-hand column. Most of the BBF samples from the IRM and ISEE 2 database earthward of $X = -19\ R_E$ are earthward. Tailward of that distance, a noticeable increase in the number of tailward samples appears in the ISEE 2 BBFs. The distributions in all three regions are off-centered in the duskward direction implying that more flow samples are pointing duskward than dawnward. Such a preference had been pointed out in the IPS slow flows of both AMPTE/IRM and ISEE 2 data sets [*Angelopoulos et al.*, 1993] and it was shown to be consistent with a diamagnetic drift of ions due to the earthward pressure gradient in the plasma sheet.

Since the BBFs can be composed of slow flows (the intervals between flow bursts) as well as fast flows (the flow bursts themselves), it is important to estimate the average speed within each sector. This is shown in the second column of Figure 6. For both IRM and ISEE 2 BBFs earthward of $X = -19\ R_E$, the average speed of the tailward flows seems to be smaller than the average speed of the earthward flows. A qualitative change in the tailward BBF samples seems to come about in the ISEE 2 BBF data set tailward of $19\ R_E$. There, the average speed of the tailward flows is larger than the average speed of the earthward flows, reminiscent of the observation of *Hones and Schindler* [1979] that at IMP 6 and IMP 8 distances the highest speed flows measured are almost all in the tailward direction.

The average speed in the duskward direction is ~200 km/s and in the dawnward direction ~150 km/s. Their difference is of the order of magnitude of the diamagnetic drifts in the center of the plasma sheet [*Angelopoulos et al.*, 1993] suggesting that a similar mechanism may also be responsible for the duskward skewedness of the BBF samples.

We can also probe the angular distribution of flows above a certain threshold, for example 400 km/s. This is shown in the third column of Figure 6. We can see that the high speed BBF samples earthward of $19\ R_E$ are predominantly earthward. However, tailward of $19\ R_E$ there is a considerable increase in the relative occurrence rate of tailward flows. Almost 20% of all ISEE 2 high speed flows in that region are within ±11.25° from the anti-sunward direction.

Although fast flows are predominantly directed along the Earth-Sun line, both earthward and tailward fast flows favor small duskward deviations from the Sun-Earth line. For example, in the ISEE 2 subset with $X < -19\ R_E$ and $|Y| < 5\ R_E$, approximately 10% of all high speed flows are centered 22.5^O away from the anti-sunward direction towards dusk, whereas approximately 20% of all fast flows are centered 22.5^O away from the sunward direction, also toward dusk. This is also consistent with the superposition of a small (~50 km/s) diamagnetic drift (due to an earthward particle pressure gradient) on the fast flow component.

5.3. Statistics of IPS Fast Flow Samples

Fast flow samples in the IPS can be studied independently of BBFs. We defined a fast earthward (tailward) flow sample as a sample with velocity greater than 400 km/s and $V_x > 0$ ($V_x < 0$). Table 1 includes the number of tailward samples (of 5-s and 12-s duration in the IRM and ISEE 2 data set, respectively) seen in the respective spatial regions. Such samples often belong to earthward BBFs (those BBFs are really of a "mixed" type, containing both earthward and tailward fast flows) both in the IRM and ISEE 2 data sets.

In an effort to link our work with the analysis of *Baumjohann et al.* [1989, 1990] that found virtually no fast tailward flows in their IRM database, we selected the tailward IRM flow samples in our AMPTE/IRM database for further investigation. We found 53 such samples in the region $-15 < X < -19\ R_E$, $|Y| < 5\ R_E$ in the IPS. Only six of these samples were accompanied by simultaneous measurements of the electron density N_e. As mentioned in section 3, our selection criteria did not require simultaneous measurements of the electron density as did the criteria used by

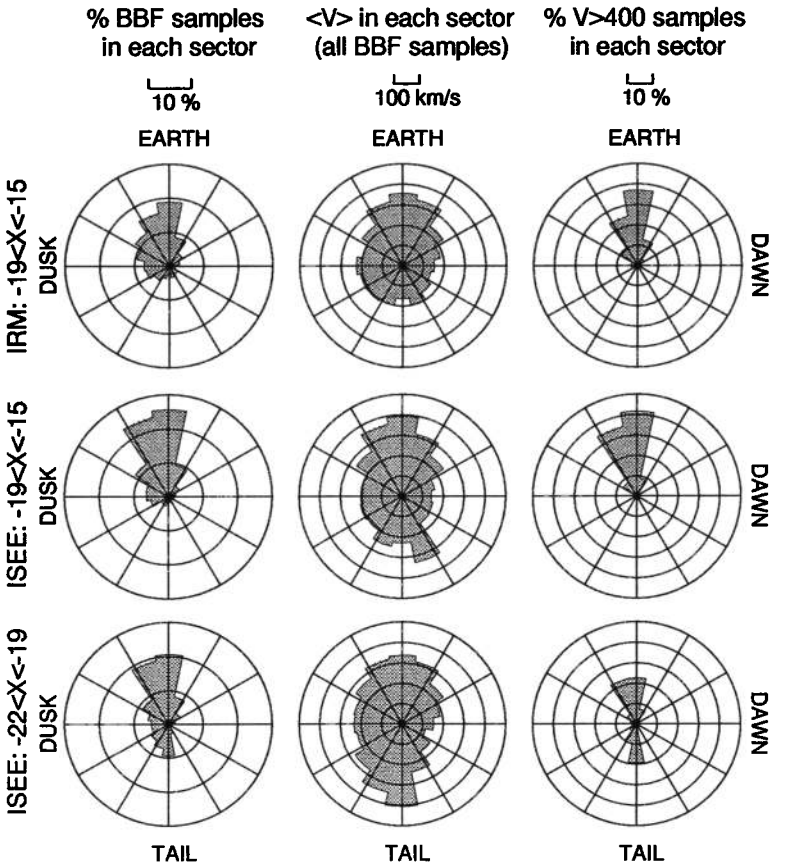

Figure 6. Sector plots of samples that comprise BBFs. The samples were segregated into three spatial regions: IRM data from 15 to 19 R_E downtail (top row), ISEE 2 data from 15 to 19 R_E downtail (middle row) and ISEE 2 data from 19 to 22 R_E downtail (bottom row). Only BBFs within $|Y_{AGSM}| < 5$ R_E were considered. The left column of the sector plots shows the percent of all BBF samples in each category whose velocity vector lies within a certain 22.5° sector. The middle column presents the average speed of the BBF samples in each sector. The right column shows the angular distribution of the samples with magnitude above 400 km/s (a subset of all BBF samples), in a similar manner as the left-most column but normalized to the total number of samples with $V_i > 400$ km/s.

Baumjohann et al. [1989, 1990]. Since our database includes samples with ion moments that are not necessarily accompanied by the (often missing) electron moments our database was significantly larger than the one used by the above authors. The observations make it clear that the majority of the fast, tailward IPS flows in our database would not have been included in the databases of *Baumjohann et al.* [1989, 1990] because of the lack of simultaneous electron measurements. Of the remaining six samples none was in the ICPS region according to the definition by *Baumjohann et al.* [1990]. Thus the few remaining samples would not have been identified as ICPS fast flows by the above authors. These observations remove an apparent contradiction between the existence of fast tailward flows in our IRM database and the lack of such flows in the earlier studies using the same satellite.

We have also studied the correlation of southward B_z with fast tailward flows. As seen on Table 1, 53% of the tailward fast flows are associated with a negative value of B_z at distances larger than 19 R_E downtail and close to midnight. Thus fast tailward flow samples correlate better with southward B_z values than tailward BBFs do.

In order to confirm our results on the relative occurrence rates of earthward and tailward BBFs and to probe the location of the first significant occurrence of fast tailward flows as the distance from Earth increases, we plot in Figure 7b the occurrence rates of fast flows in the IPS in the region $|Y_{AGSM}| < 5$ R_E. Figure 7a shows the distribution of the IPS samples in the spatial region of interest. In both plots the data have been running averaged in 1 R_E bins with a 3 R_E running box.

Fast earthward flows are more frequent in the IRM data set than in the ISEE 2 data set (Figure 7b). The same holds for the sum of earthward and tailward fast flows. In addition, fast earthward flows tend to decrease in occurrence rate tailward of ~19 R_E, whereas the sum of earthward and tailward fast flow occurrence rates tends to stabilize at about 2.5%. These results are reminiscent of the results of *Kettman et al.* [1993a, Figure 7] even though they used energetic particle anisotropies irrespective of plasma sheet region to infer the spatial dependence of the particle source's occurrence rate. Finally, as expected from our BBF analysis, tailward flows are more frequent in the ISEE 2 data set in the region of spatial overlap but such flows comprise a significant part of the entire IPS fast flow data set of the ISEE 2 mission predominantly because of the larger apogee of the satellite.

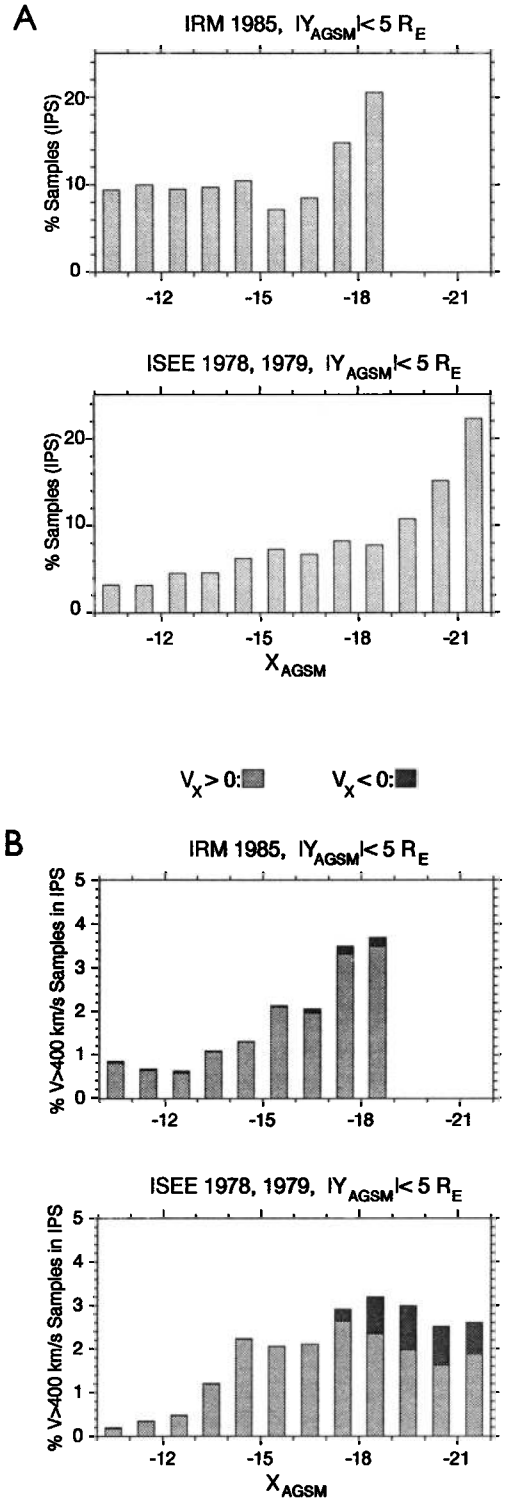

Figure 7. (a) The spatial distribution (in percent) of (top) AMPTE/IRM and (bottom) ISEE 2 IPS samples in the region $X_{AGSM} < -10\ R_E$, $|Y_{AGSM}| < 5\ R_E$, using a 3-R_E-wide running average window, centered on 1-R_E centers. (b) Occurrence rates (percent) of earthward ($V_x > 0$) fast ($V_i > 400$ km/s) flows in the IPS, denoted by the light gray-shaded bars and of tailward ($V_x < 0$) fast flows in the IPS denoted by the dark gray-shaded bars. Note that the occurrence rates of all fast flows are represented by the total height of the bar irrespective of color. The occurrence rates are running averages with a 3 R_E-wide averaging window, centered on 1 R_E bins along the X_{AGSM} direction.

6. BBF Contribution to Transport

6.1. Percent BBF Transport in the IPS

The quantity $\mathbf{f} = N_i\mathbf{V}$ represents the transport rate of particles. We can calculate the total earthward particle transport in the IPS by BBFs by integrating in time the quantity $f_x = N_i V_x$ over all BBF samples in the IPS. (This was done in the GSM coordinate system for both IRM and ISEE 2 data sets.) We can also integrate the same quantity over the entire subset of IPS samples (including BBFs) in the same spatial region of space. It is expected from previous statistical studies [*Huang and Frank*, 1986; *Baumjohann et al.*, 1989; *Angelopoulos et al.*, 1993] that the average quiet plasma sheet flow along the Earth-Sun line is earthward. Thus the ratio of the earthward BBF-related IPS particle transport f_x to the total particle transport past the satellite ought to be a number that ranges from 0 to 100%. Tailward BBFs will be excluded both from the numerator and the denominator of the above ratio because they correspond to a particular case of an "activation" region (or reconnection region) earthward of the satellite.

For earthward energy transport, the relevant quantity is the X component of the MHD energy flux density $Q = \frac{1}{2}\rho V^2 \cdot V + \frac{5}{2}(P_i + P_e)\cdot V + \frac{c}{4\pi}(E \times B)$. The electron pressure (P_e) was not readily available and was excluded from our calculations of the energy flux density, but since $T_e << T_i$ in the plasma sheet [*Baumjohann et al.*, 1989] the associated error in the evaluation of **Q** is not very large. We included all other terms that appear in the above equation. An exception was made for the Z component of the ion velocity that was not readily available from ISEE 2 and was substituted with zero in that data set. The quantity Q_x was computed in the GSM coordinate system for the IRM data set and in the GSE coordinate system for ISEE 2 data set.

In the mostly high beta IPS, to lowest order in V_x/V_S (where V_S is the sound speed in the plasma sheet), the dominant term in Q_x is P_iV_x. Thus Q_x is linearly related to V_x. Consequently, much like the equivalent quantity for f_x, the integral of Q_x over BBF samples divided by the integral of the same quantity over all IPS samples in the same region of space should be a number between 0 and 100%. We will exclude tailward BBFs from the calculation of the relative earthward transport of energy density as well.

Regarding the earthward magnetic flux transport, the relevant quantity is $E_y = -V_xB_y$. The value of E_y for both data sets was calculated from simply $-V_xB_z$ in the GSM coordinate system for IRM and the GSE coordinate system for ISEE 2. Our reason for neglecting the term V_zB_x in the calculation of E_y was twofold: first, measurements of V_z in the ISEE 2 database were not readily available; second, we recognized from inspection of the IRM data set that the level of fluctuations of V_zB_x was very large, larger than that of $-V_xB_z$, yet its average value was very small, smaller than that of $-V_xB_z$, indicating that the term V_xB_z was the crucial term in the calculation of E_y in the IPS.

Tailward high speed flows are often observed to correlate with negative B_z [e.g., *Hayakawa et al.*, 1982] in the mid-tail regions, and thus the value of E_y for those flows is positive. Occasionally this is true for the tailward BBFs in the ISEE 2 data set (see Tables 3 and 4). Flux transport during such BBFs is equivalent to earthward transport of positive (northward) magnetic flux. Because of this equivalence we will keep tailward BBFs in our database when we calculate the relative earthward magnetic flux transport accomplished by BBFs.

Plates 7 and 8 show the results of the procedure detailed above for the IRM and ISEE 2 data sets, respectively. In these plates the ratio of BBF transport to total earthward transport was calculated

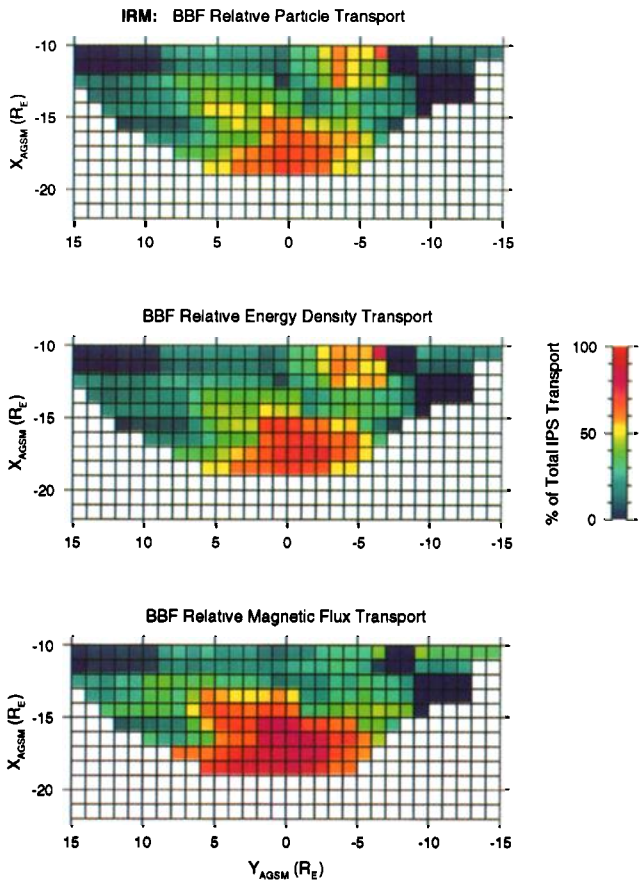

Plate 7. Percent of total measured transport past the IRM satellite that was accomplished by BBFs within a 3 x 5 R_E^2 window centered on 1 x 1 R_E^2 bins.

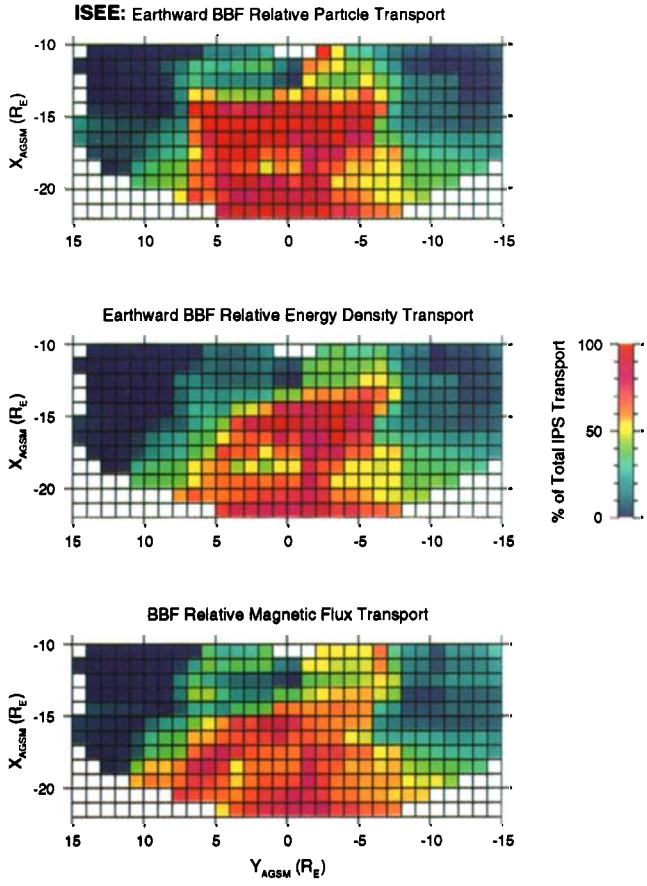

Plate 8. Same as in Plate 7 but for the ISEE 2 satellite. Tailward BBFs were excluded from the top two panels.

over a 3 x 5 R_E^2 sliding area in the X-Y direction, centered on 1 x 1 R_E^2 bins within the limits of the satellite coverage. Even if BBFs last at most 10-15% of the time in the IPS (see Plates 5 and 6), they are responsible for earthward transport of at least 30% of the total measured earthward transport in the IPS for most equatorial locations. BBFs can account for 60-100% of the transport measured past the satellites closer to apogee and at midnight, i.e., in the regions of maximum BBF occurrence rate.

The analysis presented in this section pertains to transport past the satellite location per unit cross-sectional area (in the Y-Z plane), or per unit distance (in the Y direction). An extrapolation of a single measurement of local transport to transport accomplished by the coherent flow structure that engulfs the satellite requires an estimate of the structure's size. The spatial scales associated with flows of different magnitudes are unknown. Let us suppose for a moment that one particular coherent slow flow structure of large cross-tail extent accomplishes the same earthward transport as one coherent fast flow structure of small scale size (both measured locally at different times). By comparing our local measurements we would reach the false conclusion that the fast flow is associated with more earthward transport than the slow flow. Thus for individual event studies with a single satellite, inference of the net transport based on local measurements is unwarranted.

Initially, one might think that the same argument holds for the results of a statistical analysis. However, large spatial scale flow structures would be detected by the satellite with a higher probability than small scale size flow structures. In a statistical study of a large enough database the spatial scales of the different magnitude flows weigh the occurrence frequencies of these flows. In other words, the probability of measuring a fast flow structure is proportional to the product of the probability that the structure is present anywhere in the plasma sheet times the width of the structure (normalized to an appropriate quantity like, e.g., the tail width). Therefore our statistical results concerning transport past a single point in space are expected to reflect the overall transport in the IPS. For this reason, we call the color axis of Plates 7 and 8 "% of total IPS transport," as opposed to "% transport past the spacecraft per unit Y-Z area (or per unit Y distance for magnetic flux transport) in the IPS," even though it is the latter quantity that we really measure. The results of our analysis indicate that at distances of 15-22 R_E close to midnight, most of the IPS earthward transport is accomplished over short time intervals in a bursty manner.

6.2. BBFs as Units of Transport

We now integrate with respect to time along each BBF event the earthward particle flux, energy flux density and the dawn-dusk electric field. We thus get an estimate of the total earthward transport accomplished during each event (per unit BBF cross-sectional area, or BBF Y extent). The time integrals are weakly dependent on the uncertainty in defining the BBF boundaries. BBFs are selected based on the occurrence of at least one IPS high speed flow sample within their structure. However, according to

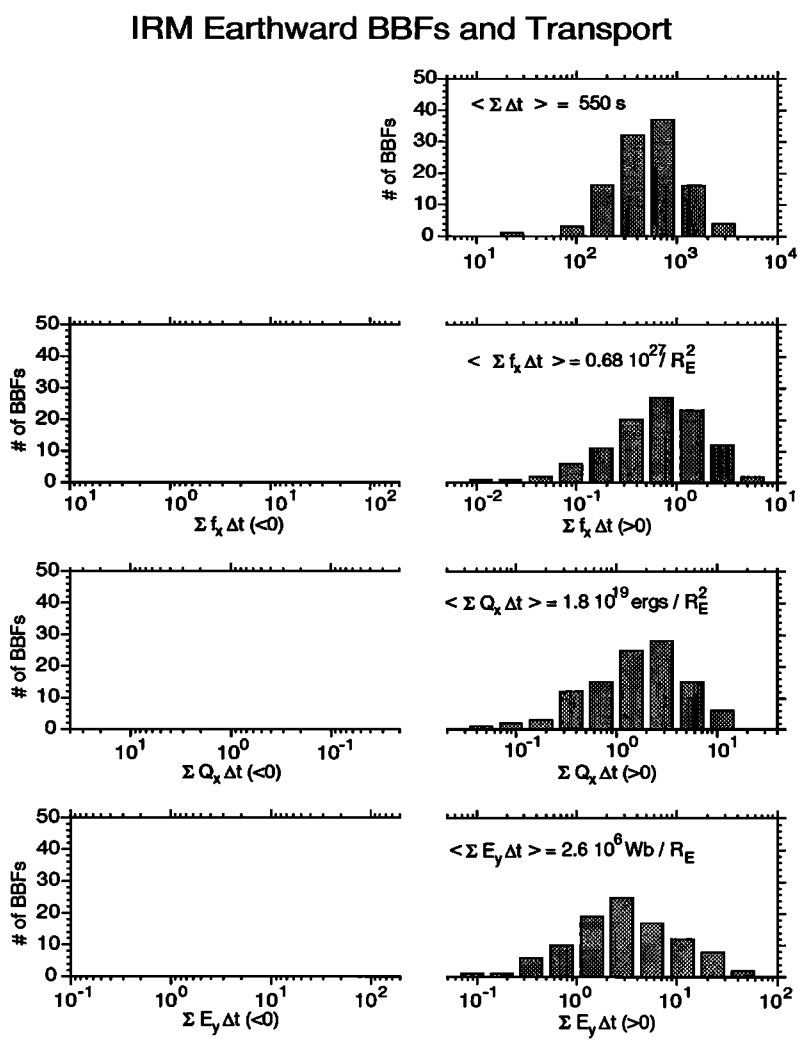

Figure 8. Histograms of the BBF duration and total transport accomplished by BBFs. From top to bottom: BBF duration in seconds; total BBF particle transport per unit Y-Z area in 10^{27} particles/ R_E^2; total BBF energy density transport per unit Y-Z area, in 10^{19} ergs/ R_E^2; magnetic flux transport per unit Y distance, in 10^6 Wb/R_E. Median values for the duration and transport are included in the panels.

their definition, BBFs are not restricted to lie entirely within the IPS. We refrained from excluding the OPS samples from the BBF structure because this would add unphysical complexity to the concept of BBFs (also see subsection titled "CPS regions" of *Angelopoulos et al.* [1992a]). As explained earlier (Section 4), most (>70%) of the BBF structure resides in the IPS. Although we excluded OPS samples when we compared BBF transport with the total transport in the IPS, we included them in our study of the BBF properties, since such samples constitute inherent parts of the BBF structure.

We present in Figure 8 the outcome of binning the earthward BBFs of the IRM database according to their duration and integral transport. The BBF distributions are fairly concentrated around the median duration and transport values indicated in each panel. Earthward BBFs from the ISEE 2 database are binned in Figure 9. The quantitative agreement between the median duration and transport values in the two data sets gives us confidence that the median values are truly representative of BBFs.

We can compare some of the median transport numbers with expected values of earthward transport of energy and magnetic flux during substorm-related intervals. The results of this comparison are presented in Table 5. During a substorm, ~2.5 x 10^{21} ergs are released on the ionosphere due to Joule heating and particle precipitation, whereas the instantaneous ionospheric power dissipation is ~4 x 10^{17} ergs/s [*Akasofu*, 1977]. Ring current dissipation is related to 10 times larger energy and power requirements than the respective ionospheric quantities [*Akasofu*, 1977]. If a substorm is the consequence of a southward IMF of 5 nT for 30 min due to a nominal 10% dayside magnetopause reconnection efficiency, then it ought to return magnetic flux of 10^8 Wb in the near-Earth region. Similar total flux transport is expected based on the rate of flux addition to the polar cap during the growth phase of substorms: *Holtzer and McPherron* [1986] give values of the order of 2. x 10^5 Wb/s for the rate of polar cap flux increase which, for a 30-min growth phase, correspond to 3.6 x 10^8 Wb of total flux added to the tail. The potential drop across the tail at active times is of the order of 100-150 kV based on an empirical formula derived from magnetotail observations [*Kivelson*, 1976, equation (11)] or based on measurements of the transpolar cap potential drop during active times [*Reiff and Luhmann*, 1986].

To evaluate the total transport accomplished by the entire

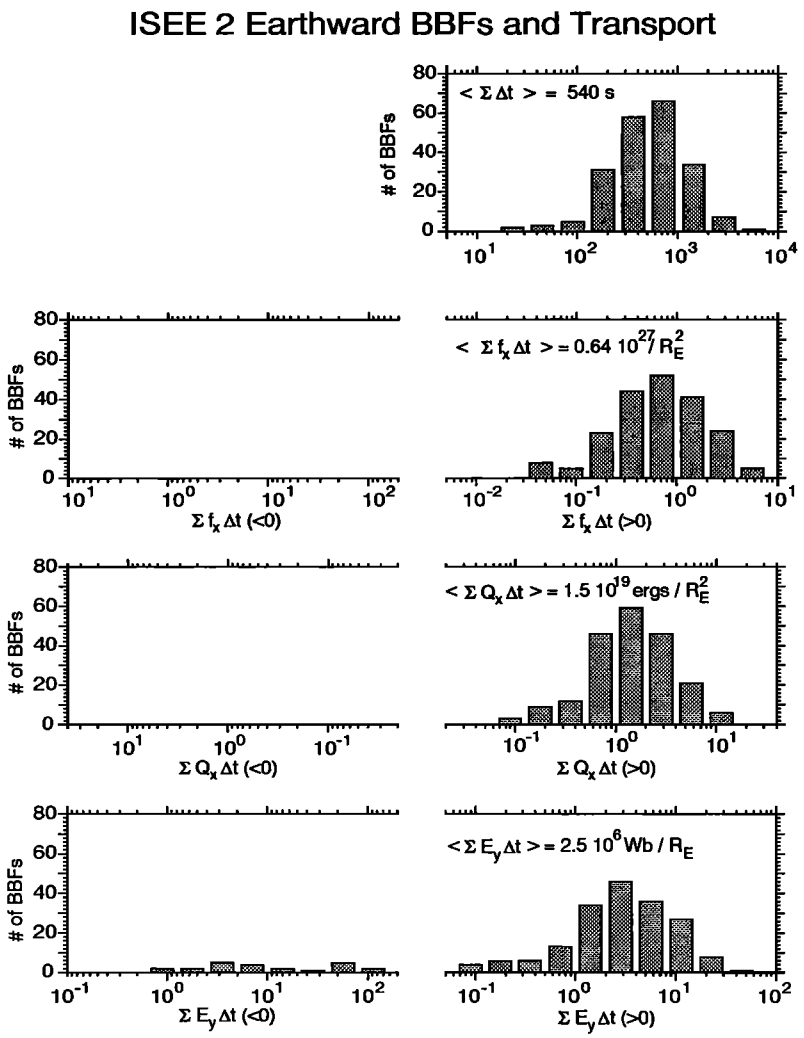

Figure 9. Same as in Figure 8 but for the earthward BBFs on the ISEE 2 satellite.

coherent flow structure of a BBF, an estimate of its scale size is needed. As noted earlier, it is not possible to determine the scale size of BBFs from single satellite measurements. For this reason we assume a reference size of 3 x 3 R_E^2 for the typical BBF and compare the substormlike transport values to the transport accomplished by a typical BBF of that reference size. It has to be stressed that the 3 x 3 R_E^2 cross-sectional area does not represent any preference based on observations or theory, but it is a mere convention. On the basis of information derived from Figures 8 and 9 (summarized in Table 5), BBFs of that size are associated with earthward magnetic flux transport of the order of 10% of the substorm-associated values quoted in the previous paragraph. The same is true for the average flux transport rate, or average electric field. The rate of energy transport during the typical BBF per 3 x 3 R_E^2 of Y-Z cross-sectional area is equivalent to the total power dissipated on the ionosphere due to Joule heating and particle precipitation, but only 10% of the total power released during substorms if the ring current (RC) contribution is included. The total BBF energy transport, is 10% of the total energy dissipated in the ionosphere during a substorm and a mere 1% of the total energy release during substorms. The reason for the factor of 10 additional deficiency in the total energy calculations relative to the power calculations is the long duration (2 hours) of the energy deposition during a substorm [*Akasofu*, 1977] relative to the short

Table 5. Comparison of BBF Transport With Expected Transport During "Typical" Substorm Conditions

QUANTITY	SUBSTORM		BBF (per Y-Z size: 3X3 R_E^2)	BBF/SUBSTORM, %	
	Ionosphere	Including RC		Ionosphere	Including RC
Power	$4.0X10^{17}$ ergs/s	$3X10^{18}$ ergs/s	$2.7X10^{17}$ ergs/s	70	10
Energy	$2.8X10^{21}$ ergs	$2.3X10^{22}$ ergs	$1.5X10^{20}$ ergs	5	1
Potential Drop	100-150 kV		14 kV	10	
Flux	$3.6X10^{8}$ Wb		$7.5X10^{6}$ Wb	2	

life span of the average BBF (10 min). Similarly, the total BBF magnetic flux transport per 3 R_E Y scale length is a mere 2% of the flux expected to circulate across the magnetosphere during a substorm.

If a single BBF event is to be associated with a substorm, and is expected to accomplish substormlike energy and magnetic flux transport rates, the numbers in Table 5 suggest that this BBF must extend across an approximately 10 times wider cross-tail width (30 R_E) than assumed. Alternatively, more than one localized BBFs, simultaneously occurring in a wide region across the tail during a single substorm could be invoked, as they would be effectively identical to a single, large-scale BBF. Paradoxically, the assumption of a wide-spread activity across the tail during every substorm is not compatible with the observations of *Hones and Schindler* [1979], who showed that at distances $-18 > X > -35$ R_E about half of the clearly defined substorms have no effect in space.

Even if we invoke spatially extended BBFs to account for substormlike energy and magnetic flux transport rates, we still cannot account for the amount of total energy deposition in the inner magnetosphere and the total flux circulation during a typical substorm by our observations in the near-Earth magnetotail. A possible resolution of this paradox may be that the observed BBF duration does not reflect the total life span of the activity in space, since a satellite can only observe one point in space. It is possible that the plasma sheet activation moves away from the satellite and persists at some other location in the tail for a duration much longer than the 10 minutes estimated from our single satellite observations.

The above comparisons of typical BBF transport with transport expected during substorms give a flavor of the issues and difficulties associated with an attempt to account for the overall energy and flux circulation in the magnetotail using single satellite measurements. Our approach is hindered by several additional problems: (1) Our database contains a multiplicity of events many of which may correspond to ionospheric activations of a smaller magnitude than our "typical" substorm. It is not clear how the average ionospheric intensification for the period under study compares with the size and duration of the "typical" substorm whose expected transport values we used in Table 5. (2) More than one BBFs may take place consecutively during a single substorm interval. Multiinstrument case studies which use measured values of the energy deposition and flux transfer during a substorm are much better suited for comparisons of the type that we attempted in this section.

A potentially important class of BBFs are the ones that occur during geomagnetically quiet times but are indistinguishable from active time BBFs based on single-point measurements in space (e.g., Figures 3 and 4). If such events are of a scale size of tens of R_E^2, then they would transport substormlike values of energy and magnetic flux earthward. Thus at least such BBFs ought to be quite localized.

Tailward BBFs from the ISEE 2 database were binned in the same manner as earthward ones and the results are shown in Figure 10. Tailward BBFs are, on the average, of shorter duration than earthward BBFs. There are indications that the plasma sheet is thin during tailward near-neutral sheet flow events: Such flows are only observed at small distances from the expected neutral sheet position (Plates 5 and 6, Tables 2, 3, and 4) and while they last the magnetic field is most often taillike (e.g., Figure 3). It is possible that the average duration and transport of tailward BBF events is spatially aliased, as the satellite may not remain long enough in the plasma sheet to detect the full temporal growth and evolution of a tailward flow event. In addition, their small number does not necessarily warrant a statistical treatment, thus it is not clear whether the medians in Figure 10 are truly representative of such events.

In agreement with the contents of Tables 2, 3, and 4 (discussed in section 5.1) it is apparent from Figure 10 that most of the tailward BBFs in the ISEE 2 database are associated with a negative average E_y. Although the method used to calculate the value of E_y is not strictly consistent with MHD (we assumed $V_Z = 0$), this result suggests that most tailward BBFs are associated with tailward transport of closed magnetic flux. Of the 47 (13) tailward BBFs in the ISEE-2 (IRM) data set only 18 (3) were associated with an average southward B_Z. The small plasma sheet thickness during tailward flow events, and the possibility of existence of multiple, localized acceleration centers during a geomagnetically active period can add significantly to the complexity in interpretation of the above results.

7. Summary and Discussion

We analyzed BBF events as units of transport in the inner plasma sheet, using data from the AMPTE/IRM and ISEE 2 satellites. Applying a common methodology for region identification and event selection, we studied the BBF properties. We tried to explain the differences in BBF properties in the data sets from the two satellites based on the satellites' orbital characteristics and geomagnetic conditions. Possible instrumental differences cannot be ruled out as contributors to the observed differences, but they were not explored in this paper. We conveniently used the distance of $X = -19$ R_E, the AMPTE/IRM apogee, as a spatial divider of the ISEE 2 data set in order to pursue comparisons both between the ISEE 2 and IRM data set in the region of spatial "overlap" ($-15 < X < -19$, $|Y| < 5$) and between two spatial regions (tailward and earthward of that distance) from the ISEE 2 satellite. Our results are as follows:

7.1. BBF Occurrence Rates

(1) Earthward BBFs $(\overline{V}_x > 0)$ have a spatial occurrence rate in the IPS that increases with proximity to midnight and distance from Earth up to $X = -19$ R_E (Plates 5 and 6). This is in agreement with the results of *Baumjohann et al.* [1989, 1990] on the occurrence rates of fast flows in the plasma sheet. It is not certain whether the dependence of the BBF occurrence frequency on distance from Earth is an artifact of our selection criterion that $V_i > 400$ km/s. In particular, if BBF-related earthward transport of magnetic flux is responsible for the flux return in the near-Earth regions it ought to continue at the same occurrence rate in the near-Earth environment. The lack of BBFs at these regions may suggest either that the transport is taking place in a qualitatively different manner, i.e., by slow, non bursty flows, or that the BBF peak amplitude decreases below our arbitrary 400 km/s criterion for BBFs earthward of 15 R_E. This could happen if the value of the equatorial B_z were to increase with proximity to Earth since a smaller earthward flow velocity would be necessary for transport of the same amount of magnetic flux earthward. However, the value of the equatorial B_z decreases slightly as the distance from Earth decreases from $X_{GSM} = -25$ to $X_{GSM} = -15$ R_E according to an empirical model of the tail's magnetic field [*Stern and Tsyganenko*, 1992]. It is only inside of $X = -13$ R_E that B_Z increases rapidly beyond its value at $X = -25$ R_E suggesting that the decrease in the occurrence rate of BBFs from 22 to 13 R_E downtail may not be attributable to the above flux conservation argument.

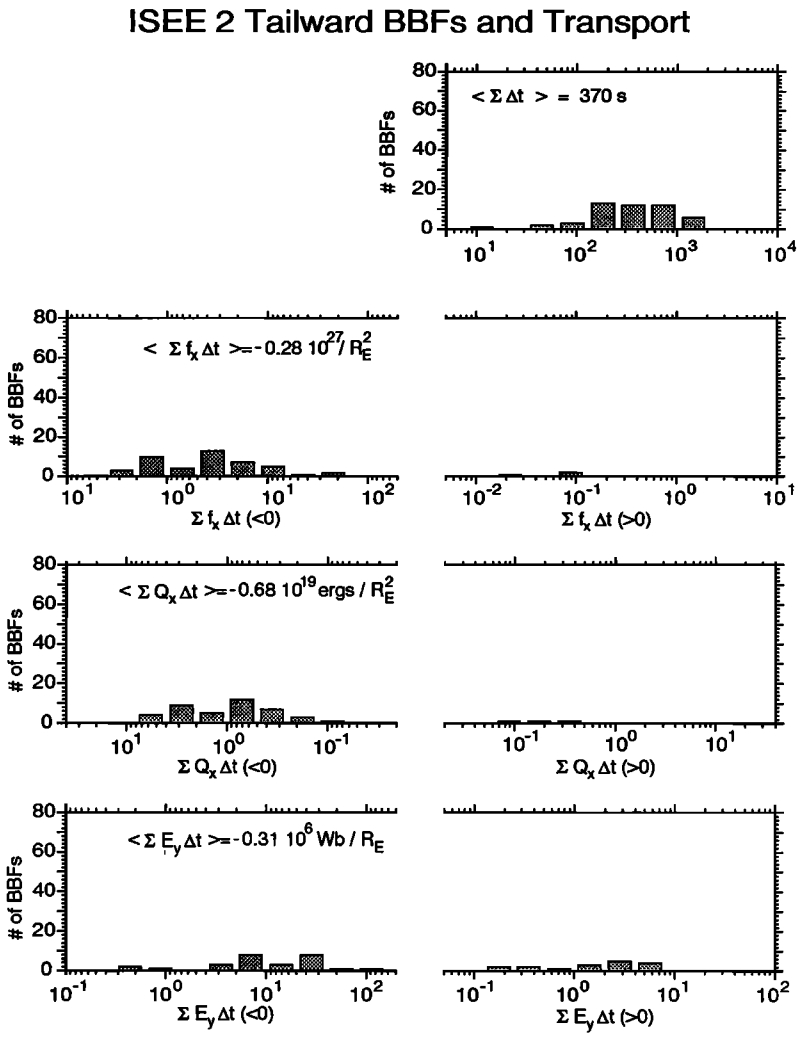

Figure 10. Same as in Figure 9 but for the tailward BBFs on the ISEE 2 satellite.

(2) Earthward BBFs are more frequent in the IRM database than in the ISEE 2 database in the region of overlap (Plates 5 and 6). The same holds for the union of the earthward and tailward BBF subsets (Figure 5). Both results are supported by an independent analysis of fast flow samples in the IPS.

A possible explanation for this difference may be that deducing the occurrence rate of BBFs may not be as simple an operation as a normalization of the BBF duration by the time spent by the satellite in the IPS. It is possible that plasma sheet reconfigurations during BBFs coupled with the different distances of the two satellites from the expected neutral sheet position may influence the observed occurrence rates. It is not possible to address this problem without a good understanding of such reconfigurations, a task that demands multisatellite studies of carefully selected events.

(3) Tailward of X = -19 R_E the earthward BBF occurrence rate decreases as the total (earthward plus tailward) BBF occurrence rate stabilizes in the ISEE 2 data set. The same behavior of the occurrence rates is also evident in an independent analysis of the fast flow samples in the IPS (Figure 6).

Again, it is difficult to understand this result. We note, however, that it is supported by the study of *Kettmann et al.* [1993a Figure 7) that shows a similar decrease in earthward energetic anisotropies tailward of X = -17 R_E. Since the satellite and time period used in this study is the same as the one used by the above authors, it is likely that the observed decrease of occurrence rates may be due to the same reason. As the distance from the expected neutral sheet location increases with distance from Earth for the inclined ISEE 2 orbit, it is possible that, as discussed earlier, this adds complexity in the determination of the occurrence rates that cannot be removed by a simple division of the observed BBF duration by the total IPS observation time.

7.2. Tailward BBFs

(1) Tailward BBFs are very infrequent in the IRM database and somewhat less infrequent in the ISEE 2 database earthward of X= -19 R_E. The local time distribution of tailward BBFs in both data sets can be understood on the assumption that the plasma sheet is thin during observations of fast tailward flows. The difference between the occurrence rates of tailward BBFs in the IRM and ISEE 2 data sets in the region of spatial overlap can be attributed to the quieter geomagnetic conditions prevailing in the IRM data set relative to the ISEE 2 data set (Table 1). Tailward BBFs are most frequent tailward of X= -19 R_E and close to midnight.

(2) The few tailward BBFs (and high speed tailward flows) in our AMPTE/IRM near-neutral sheet data set were not reported by *Baumjohann et al.* [1990] predominantly because these authors

used an approximately 42% smaller data set than we did. Secondarily, they are due to the different identifier of proximity to the neutral sheet (we defined the IPS based on plasma beta, whereas *Baumjohann et al.* [1989] defined the ICPS based on the magnetic field magnitude and elevation).

(3) The percentage of all BBFs observed that are tailward increases with distance downtail out to ISEE-2 apogee. The ratio of tailward to all fast flows increases with distance from Earth. Comparison of our results from Table 1 and the results of *Hayakawa et al.* [1982] and *Nakamura et al.* [1994] suggests that this ratio continues to increase out to X = -30 R_E downtail.

7.3. Tailward BBFs and B_z

(1) Most tailward BBFs have a northward average B_z and are consequently associated with an average electric field in the dusk-to-dawn direction. The correlation of fast tailward flows and southward B_z is better, though, supporting our observation that it is the transient nature of the southward B_z turnings during BBFs that is causing the average B_z during most BBFs to be positive. (Tailward of X=-19 R_E and within 5 R_E from the midnight plane only ~45% of the tailward BBFs are associated with a positive E_y, whereas 53% of all fast tailward flows are associated with a positive B_z.) Spatial aliasing due to small plasma sheet thicknesses as well as multiple acceleration centers may be possible explanations for these observations.

(2) The percentage of tailward BBFs that correlate positively with southward B_z increases with increasing distance from Earth (Tables 2, 3, and 4), as does the percentage of fast tailward flows that obeys the same correlation. As such a correlation becomes increasingly better out to distance of X~-30 R_E [*Hayakawa et al.*, 1982; *Nakamura et al.*, 1994] it is possible that the geometry of a neutral line does not attain its macroscopic topology prescribed by MHD until further downstream from the region where fast tailward flows are detectable first.

7.4. Location of Near-Earth Neutral Line

A determination of the earthward-most location of the origin of the tailward flows is more complex than the present study. The thinness of the plasma sheet during tailward flow events, the small local time extent of the initial perturbation that may be responsible for such flows, the possible transient nature of the tailward flows, the dependence of the location and duration of the tailward flows on activity and the possibility of multiple substorm onsets makes such an endeavor extremely difficult with one satellite measurements [*McPherron et al.*, 1993]. Our result that the ratio of tailward to earthward fast flow occurrence rates starts becoming measurable anywhere between 15 and 19 R_E downtail suggests that such a distance is probably an upper limit to the distance at which such flows may be generated at active times.

However, it must be stressed that the answer to the question "what is the most probable location of a near-Earth neutral line?" depends on the way this question is implemented in the analysis of the data. While tailward flows become a quite significant (30%) portion of all fast flows at distances 19-21 R_E downtail, such flows are most often not threaded by southward B_z fields within the ISEE 2 apogee, something that may explain the different answers given to the above question by *Kettmann et al.* [1993a] and *Cattell and Mozer* [1984].

7.5. BBF Importance for Magnetotail Transport

Even if BBFs last for a relatively short time in the IPS (7-15% at apogee and close to midnight) they are responsible for most of the measured transport of mass, energy and northward directed magnetic flux toward Earth (60-100% in the regions of maximum occurrence rate). Thus they represent the predominant mechanism of earthward convection at distances of 15-22 R_E and close to midnight.

7.6. "Typical" BBF Duration and Integral Transport

The median earthward BBF duration is ~550 s, whereas the median BBF particle, energy and magnetic flux transport past the satellite is $0.65\times10^{27} R_E^{-2}$, 1.5×10^{19} ergs/R_E^2, and 2.5×10^{6} Wb/R_E, respectively. The similarity of the median values of the duration and transport characteristics of earthward BBFs in the two databases is an indication that the median transport numbers are truly representative of the "typical" BBF.

BBFs were selected under the assumption that flow bursts that were less than 10 min apart belong to the same BBF event. This was based on our visual inspection of BBFs and the perception that not only temporal but also spatial effects are responsible for the variability of the flow velocity. Thus the histograms of BBF durations (Figures 8, 9) should be biased towards BBFs that are longer than 10 min. However, the median earthward BBF duration in both data sets is about 10 min indicating that our assumption does not influence the duration of BBFs significantly.

As the occurrence rate of BBFs increases with geomagnetic activity we expect that active time BBFs are a dominant class of BBFs in our databases. Yet, despite their important significance for the total earthward transport measured past the spacecraft, BBFs have median values of energy and magnetic flux transport rates that are only 10% of the expected values during magnetospheric substorms, per 3 x 3 R_E^2 BBF cross-sectional area in the Y-Z plane (although their energy transport rate is sufficient to power ionospheric dissipation during substorms). The integral energy and magnetic flux transport per 3 x 3 R_E^2 BBF size is only 1-2% of the total energy deposition and flux transfer during substorms (Table 5). Thus if a single BBF is to be associated with a typical substorm, not only does it have to occupy a significant crosssection of the magnetotail at active times, but in addition it will have to last several times longer than its median observed duration of 10 min. The occasional lack of fast flows in the plasma sheet during geomagnetically active periods *[Hones and Schindler,* 1979] is incompatible with the above scenario, in which a large cross-sectional area and long duration BBF should always be seen sometime, somewhere in space in association with a substorm.

This apparent paradox can only be resolved by case studies of BBFs and their association with substorms. Such studies should employ multiple satellites in order to diagnose as completely as possible the substorm onset and its evolution. Solar wind data and ground observables (Dst) would be necessary to determine the solar wind energy and flux transport during growth phase and the energy and magnetic flux release during and after expansion onset. Coordinated Data Analysis Workshop (CDAW)-type analyses of BBF events can also further our understanding of the apparent lack of one-to-one relationship between BBFs and geomagnetic activity as determined by the AE index [*Angelopoulos et al.*,

1992a]. Spatial aliasing due to plasma sheet flapping and crude AE station deployment may be possible reasons for the lack of such an apparent correlation.

Acknowledgments. V.A. thanks the SST-7 and SST-9 groups of LANL for their hospitality during the completion of part of this work and for stimulating discussions. We would like to thank C. M. Hammond for his help with the aberration of the position data. Useful discussions with K. Khurana, C. M. Hammond, D. H. Fairfield and C. A. Cattell are gratefully acknowledged. V.A. and C.F.K. were supported by grants NSF ATM 91-20591 and LANL/UCRP 304. F.V.C. and R.P. were supported by NASA grant NAGW 2620. M.G.K. was supported by NSF grant ATM 91-15557. R.J.W. was supported by NASA grant NAG 5-1530. C.T.R. was supported by NAG5-1967.

The Editor thanks E. F. Donovan and P. Song for their assistance in evaluating this paper.

References

Akasofu, S.-I., *Physics of Magnetospheric Substorms*, p. 274, D. Reidel, Norwell, Mass., 1977.

Angelopoulos, V., W. Baumjohann, C. F. Kennel, F. V. Coroniti, M. G. Kivelson, R. Pellat, R. J. Walker, H. Lühr, and G. Paschmann, Bursty bulk flows in the inner central plasma sheet, *J. Geophys. Res., 97*, 4027, 1992a.

Angelopoulos, V., C. F. Kennel, F. V. Coroniti, R. Pellat, M. G. Kivelson, R. J. Walker, W. Baumjohann, G. Paschmann, and H. Lühr, Bursty bulk flows in the inner plasma sheet: An effective means of earthward transport in the magnetotail, in *Proceedings of the First International Conference on Substorms, Eur. Space Agency Spec. Publ., ESA SP-335*, 303-308, 1992b.

Angelopoulos, V., C. F. Kennel, F. V. Coroniti, R. Pellat, H. E. Spence, M. G. Kivelson, R. J. Walker, W. Baumjohann, W. C. Feldman, J. T. Gosling, and C. T. Russell, Characteristics of ion flow in the quiet state of the inner plasma sheet, *Geophys. Res. Lett., 20*, 1711-1714, 1993.

Bame, S. J., J. Asbridge, H. E. Felthauser, J. P. Glore, G. Paschmann, P. Hemmerich, K. Lehmann, and H. Rosenbauer, ISEE-1 and ISEE-2 fast plasma experiment and the ISEE-1 solar wind experiment, *IEEE Trans. Geosci. Electron., GE-16*, 216-220, 1978.

Baumjohann, W., The near-Earth plasma sheet: An AMPTE/IRM perspective, *Space Sci. Rev., 64*, 141-163, 1993.

Baumjohann, W., G. Paschmann, N. Sckopke, C. A. Cattell, and C. W. Carlson, Average ion moments in the plasma sheet boundary layer, *J. Geophys. Res., 93*, 11507-11520, 1988.

Baumjohann, W., G. Paschmann, and C. A. Cattell, Average plasma properties in the central plasma sheet, *J. Geophys. Res., 94*, 6597-6606, 1989.

Baumjohann, W., G. Paschmann, and H. Lühr, Characteristics of high-speed ion flows in the plasma sheet, *J. Geophys. Res., 95*, 3801-3809, 1990.

Cattell, C. A., and R. C. Elphic, Comment on "A statistical study of the central plasma sheet: Implications for substorm models" by C. Y. Huang and L. A. Frank, *Geophys. Res. Lett., 14*, 773-775, 1987.

Cattell, C. A., and F. S. Mozer, Substorm electric fields in the Earth's magnetotail, in *Magnetic Reconnection in Space and Laboratory Plasmas, Geophys. Monogr. Ser.*, vol. 30, edited by E. W. Hones Jr., pp. 208-215, AGU, Washington, D. C. 1984.

Chen, S.-H., and M. G. Kivelson, On ultralow frequency waves in the lobes of the Earth's magnetotail, *J. Geophys. Res., 96*, 15711-15723, 1991.

Eastman, T. E., L. A. Frank, and C. Y. Huang, The boundary layers as the primary transport regions of the Earth's magnetotail, *J. Geophys. Res., 90*, 9541-9560, 1985.

Garrett, H. B., The charging of spacecraft surfaces, *Rev. Geophys., 19*, 577-616, 1981.

Hammond, K. M., M. G. Kivelson, and R. J. Walker, Imaging the effect of dipole tilt on magnetotail boundaries, *J. Geophys. Res., 99*, 6079-6092, 1994.

Harris, E. G., On a plasma sheath separating regions of oppositely directed magnetic field, *Nuovo Cimento Soc. Ital. Fis. A, 23*, 115-120, 1962.

Hayakawa, H., A. Nishida, E. W. Hones Jr., and S. J. Bame, Statistical characteristics of plasma flow in the magnetotail, *J. Geophys. Res., 87*, 277-283, 1982.

Holtzer, R. E., and R. L. McPherron, A quantitative empirical model of the magnetospheric flux transfer processes, *J. Geophys. Res., 91*, 3287-3293, 1986.

Hones, E. W., Jr., Plasma flow in the magnetotail and its implications for substorm theories, in *Dynamics of the Magnetosphere*, edited by S.-I. Akasofu, D. Reidel Pub. Co., Dordrecht, Holland, pp. 545-562, 1979.

Hones, E. W., Jr. and K. Schindler, Magnetotail plasma flow during substorms: A survey with IMP 6 and IMP 8, *J. Geophys. Res., 84*, 7155-7169, 1979.

Hones, E. W., Jr., T. A. Fritz, J. Birn, J. Cooney, and S. J. Bame, Detailed observations of the plasma sheet during a substorm on April 24, 1979, *J. Geophys. Res., 91*, 6845-6859, 1986.

Huang, C. Y., and L. A. Frank, A statistical study of the central plasma sheet: Implications for substorm models, *Geophys. Res. Lett., 13*, 652-655, 1986.

Huang, C. Y., and L. A. Frank, Reply to Cattell and Elphic, *Geophys. Res. Lett., 14*, 776-778, 1987.

Huang, C. Y., L. A. Frank, and T. E. Eastman, Plasma flows near the neutral sheet of the magnetotail, in *Magnetotail Physics*, edited by A. T. Lui, pp. 127-135, Johns Hopkins University Press, Baltimore, Md., 1987.

Kettmann, G., T. A. Fritz, E. W. Hones, Jr., and P. W. Daly, Energetic ion anisotropies in the geomagnetic tail, 1, A statistical survey, *J. Geophys. Res., 98*, 99-113, 1993a.

Kettmann, G., T. A. Fritz, E. W. Hones Jr., and P. W. Daly, Energetic ion anisotropies in the geomagnetic tail, 2, Magnetic field and substorm characteristics, *J. Geophys. Res., 98*, 115-129, 1993b.

Kivelson, M. G., Magnetospheric electric fields and their variation with geomagnetic activity, *Rev. Geophys., 14*, 189-197, 1976.

Lühr, H., N. Klöcker, W. Oelschlägel, B. Häusler, and M. Acuña, The IRM fluxgate magnetometer, *IEEE Trans. Geosci. Remote Sens., GE-23*, 259-261, 1985.

Mauk, B. H., and C.-I. Meng, Plasma injection during substorms, *Phys. Scr., 18*, 128-139, 1987.

McPherron, R. L., Physical processes producing magnetospheric substorms and magnetic storms, *Geomagnetism, 4*, 593-739, 1991.

McPherron, R. L., V. Angelopoulos, D. N. Baker, and E. W. Hones Jr., Is there a near-Earth neutral line?, *Adv. Space. Res., 13*, 173-186, 1993.

Nakamura, R., D. N. Baker, D. H. Fairfield, D. G. Mitchell, R. L. McPherron, E. W. Hones, Jr., Plasma flow and magnetic field characteristics near the midtail neutral sheet, *J. Geophys. Res., accepted*, 1994.

Nishida, A., H. Hayakawa, and E. W. Hones Jr., Observed signatures of reconnection in the magnetotail, *J. Geophys. Res., 86*, 1422-1436, 1981.

Ohtani, S., R. C. Elphic, C. T. Russell, and S. Kokubun, ISEE-1 and -2 observations of an isolated diamagnetic event: An earthward-moving plasma bulge or a tail-aligned flux rope?, *Geophys. Res. Lett., 19*, 1743-1746, 1992.

Paschmann, G., H. Loidl, P. Obermayer, M. Ertl, R. Laborenz, N. Sckopke, W. Baumjohann, C. W. Carlson, and D. W. Curtis, The plasma instrument for AMPTE/IRM, *IEEE Trans. Geosci. Remote Sens., GE-23*, 262-266, 1985a.

Paschmann, G., N. Sckopke, and E. W. Hones Jr., Magnetotail plasma observations during the 1054 UT substorm on March 22, 1979 (CDAW 6), *J. Geophys. Res., 90*, 1217-1229, 1985b.

Reiff, P. H., and J. G. Luhmann, Solar wind control of the polar-cap voltage, in *Solar Wind-Magnetosphere Coupling*, edited by Y. Kamide and J. Slavin, p. 453, Terra Scientific, Tokyo, 1986.

Russell, C. T., The ISEE-1 and -2 magnetometers, *Geosci. Electron., 16*,

239-242, 1978.

Sergeev, V. A., R. C. Elphic, F. S. Mozer, A. Saint-Marc, and J. A. Sauvaud, A two-satellite study of nightside flux transfer events in the plasma sheet, *Planet. Space Sci., 40,* 1551-1572, 1992.

Stern, D. P., and N. A. Tsyganenko, Uses and limitations of the Tsyganenko magnetic field models, *EOS Trans., AGU, 73,* 489, 493-494, 1992.

V. Angelopoulos, Applied Physics Laboratory, Johns Hopkins University, Johns Hopkins Rd., Laurel, MD 20723-6099. (e-mail: vassilis@jhuapl.edu)

W. Baumjohann, Max-Planck-Institut für Extraterrestrische Physik, D-8046, Garching, Germany.

F. V. Coroniti, C. F. Kennel, and R. Pellat, Department of Physics, University of California at Los Angeles, Los Angeles, CA 90024.

W. C. Feldman and J. T. Gosling, Los Alamos National Laboratory, MS D-466, Los Alamos, NM 87545.

M. G. Kivelson, C. T. Russell and R. J. Walker, Institute of Geophysics and Planetary Physics, University of California at Los Angeles, Los Angeles, CA 90024.

(Received November 15, 1993; revised April 13, 1994; accepted May 11, 1994.)